

## Research



**Cite this article:** Briant LJB, Zhang Q, Vergari E, Kellard JA, Rodriguez B, Ashcroft FM, Rorsman P. 2017 Functional identification of islet cell types by electrophysiological fingerprinting. *J. R. Soc. Interface* **14**: 20160999.  
<http://dx.doi.org/10.1098/rsif.2016.0999>

Received: 9 December 2016

Accepted: 15 February 2017

**Subject Category:**

Life Sciences—Mathematics interface

**Subject Areas:**

computational biology, biophysics,  
biomathematics

**Keywords:**

islet electrophysiology, logistic regression,  
 $\alpha$ -cell,  $\beta$ -cell,  $\delta$ -cell, conductance-based  
models

**Author for correspondence:**

Linford J. B. Briant

e-mail: [linford.briant@ocdem.ox.ac.uk](mailto:linford.briant@ocdem.ox.ac.uk)

## Functional identification of islet cell types by electrophysiological fingerprinting

Linford J. B. Briant<sup>1,2</sup>, Quan Zhang<sup>1</sup>, Elisa Vergari<sup>1</sup>, Joely A. Kellard<sup>1</sup>, Blanca Rodriguez<sup>2</sup>, Frances M. Ashcroft<sup>3</sup> and Patrik Rorsman<sup>1,4</sup>

<sup>1</sup>Oxford Centre for Diabetes, Endocrinology, and Metabolism, Radcliffe Department of Medicine, University of Oxford, Churchill Hospital, Oxford OX3 7LE, UK

<sup>2</sup>Department of Computer Science, University of Oxford, Oxford OX1 3QD, UK

<sup>3</sup>Department of Physiology, Anatomy, and Genetics, University of Oxford, South Parks Road, Oxford OX1 3PT, UK

<sup>4</sup>Metabolic Research, Department of Physiology, Institute of Neuroscience and Physiology, University of Göteborg, SE-405 30 Göteborg, Sweden

LJB, 0000-0003-3619-3177

The  $\alpha$ -,  $\beta$ - and  $\delta$ -cells of the pancreatic islet exhibit different electrophysiological features. We used a large dataset of whole-cell patch-clamp recordings from cells in intact mouse islets ( $N = 288$  recordings) to investigate whether it is possible to reliably identify cell type ( $\alpha$ ,  $\beta$  or  $\delta$ ) based on their electrophysiological characteristics. We quantified 15 electrophysiological variables in each recorded cell. Individually, none of the variables could reliably distinguish the cell types. We therefore constructed a logistic regression model that included all quantified variables, to determine whether they could together identify cell type. The model identified cell type with 94% accuracy. This model was applied to a dataset of cells recorded from hyperglycaemic  $\beta$ V59M mice; it correctly identified cell type in all cells and was able to distinguish cells that co-expressed insulin and glucagon. Based on this revised functional identification, we were able to improve conductance-based models of the electrical activity in  $\alpha$ -cells and generate a model of  $\delta$ -cell electrical activity. These new models could faithfully emulate  $\alpha$ - and  $\delta$ -cell electrical activity recorded experimentally.

## 1. Introduction

The pancreatic islet is composed of three main cell types:  $\alpha$ -,  $\beta$ - and  $\delta$ -cells [1,2]. All three cell types are electrically excitable and use electrical signals to regulate hormone release [3–5]. These hormones—glucagon, insulin and somatostatin, respectively—all have a role in normalizing plasma glucose [6–8]. In type 2 diabetes mellitus (T2DM), both glucagon and insulin secretion are impaired [9,10]. This impairment has been linked to changes in the electrical properties of  $\alpha$ - and  $\beta$ -cells [11–14]. Determining the mechanisms by which islet cells couple electrical activity to hormone secretion is therefore fundamental for understanding normal glucose homeostasis and the pathophysiology of T2DM.

The whole-cell patch-clamp technique, applied to intact islets, is the perfect experimental paradigm for understanding the electrophysiological properties of islet cells. However, within a mouse islet, the different cell types are not present in equal proportions;  $\beta$ -cells are the most abundant (70–80% of all cells), with  $\alpha$ -cells (15–20%) and  $\delta$ -cells (5–10%) being relatively sparse [15]. Thus, whereas there have been great advances in our understanding of the electrical properties of  $\beta$ -cells and how they couple to insulin secretion in both health and disease [16–18], progress has been slower and shrouded in controversy for  $\alpha$ -cells [4,19–21]. For  $\delta$ -cells, there remains great uncertainty, even with regard to fundamental aspects of the metabolic regulation of their electrical activity.

This has motivated the development of strategies to improve identification of islet cell type.  $\beta$ -cells can be separated from non- $\beta$ -cells by autofluorescence-activated cell sorting [22]. Although this can purify  $\beta$ -cells and  $\alpha$ -cells by

80–90%, it has the drawback of removing cells from their paracrine environment—an environment necessary for maintaining normal electrophysiological and secretory function [8,23–27]. Recent efforts have been made to produce fluorescent labels for particular islet cell types in the mouse [28–30]. However, it is not straightforward to distinguish labelled and non-labelled cells in the intact islet owing to fluorescence emission from cells deeper in the tissue layer. For this reason, islet cells from such transgenic mice are often dispersed into single cells [29,31–33]. This allows labelled cells to be identified, but again removes them from their paracrine environment. Many experiments are therefore still performed on intact islets harvested from normal (i.e. not genetically modified) mice, where cell type must be distinguished by reference to established differences in the electrophysiological properties of  $\alpha$ -,  $\beta$ - and  $\delta$ -cells or post-recording, using immunocytochemistry. Here, we explored whether the electrophysiological properties can be used to reliably ‘functionally identify’ each cell type.

Currently, electrophysiological identification of cell type ( $\alpha$ ,  $\beta$  or  $\delta$ ) relies on two criteria. The first is that  $\beta$ -cells are larger than non- $\beta$ -cells [3,34–44]. The second is that  $\alpha$ -,  $\beta$ - and  $\delta$ -cells possess distinct ionic channels or similar channels that exhibit different properties. For example,  $\beta$ -cells exhibit non-inactivating  $K^+$  currents and a voltage-gated  $Na^+$  current that inactivates at very hyperpolarized potentials [37,39,45]. In contrast, there is evidence that non- $\beta$ -cells express an A-type transient  $K^+$  current [29,31,38,46–48], a  $Na^+$  current with depolarized inactivation properties relative to the  $\beta$ -cell [11,29,39–41,44–47,49,50] and T-type  $Ca^{2+}$  channels [3,38,46]. Several laboratories have used these different electrophysiological fingerprints to distinguish between  $\alpha$ -,  $\beta$ - and  $\delta$ -cells [11,13,31,34–36,39–44,46–48,50–53].

Here we reviewed the electrophysiological fingerprints of mouse  $\alpha$ -,  $\beta$ - and  $\delta$ -cells. We recorded and analysed a large dataset of whole-cell voltage-clamp recordings (288 recordings) made from cells in intact mouse islets, whose cell type was subsequently unequivocally determined by immunocytochemistry. We used these data to investigate the validity of these properties for cell identification and to produce a mathematical model for identifying islet cell type. We show that this model can reliably identify islet cell type and can be successfully used to monitor transdifferentiation of cells in a diabetic mouse model ( $\beta V59M$ ) [54]. Our findings demonstrate that the electrophysiological properties of  $\alpha$ - and  $\delta$ -cells differ somewhat from what has previously been deduced. We finally used this amended information to improve reported conductance-based models of the electrical activity in  $\alpha$ -cells and  $\delta$ -cells and show that these revised models faithfully resemble experimentally recorded action potential shape.

## 2. Methods

### 2.1. Animals used in this study

Recordings from 288 cells in islets from five different strains of mouse with a normoglycaemic phenotype were used in this study. The mouse strains were NMRI, C57BL/6, EPAC2-KO [55], GYY [32] and SST-Cherry [56]. Islets from a mouse model with a hyperglycaemic phenotype were also used, together with littermate controls [54]. These mice have a valine-to-methionine substitution in the Kir6.2 subunit of the ATP-sensitive  $K^+$  ( $K_{ATP}$ )

channel in  $\beta$ -cells ( $\beta V59M$  mice). This dataset consisted of 13 recordings from  $\beta V59M$  mice, and 15 from littermate controls.

### 2.2. Preparation of pancreatic islets

Mice were killed by cervical dislocation, and islets isolated by liberase digestion (schedule 1 procedure). Islets were used for acute experiments and were not maintained in tissue culture for less than 16 h. A new islet was used for each cell recording.

### 2.3. Whole-cell patch-clamp recordings

Whole-cell currents were recorded in intact islets using the standard whole-cell configuration. Measurements were performed using an EPC-10 patch-clamp amplifier and PULSE software (HEKA Electronics, Lambrecht/Pfalz, Germany). Currents were filtered at 2.9 kHz and digitized at more than 10 kHz. Currents were compensated for capacitive transients and leak current subtraction was conducted. The extracellular medium consisted of (mM) 118 NaCl, 20 tetraethylammonium-Cl (TEA-Cl), 5.6 KCl, 1.2  $MgCl_2$ , 5 HEPES (pH 7.4 with NaOH), 2.6  $CaCl_2$  and 1 D-glucose. Two intracellular (pipette) solutions were used (solution 1 and solution 2). Solution 1 contained (mM) 125 K-glut, 10 KCl, 10 NaCl, 1  $MgCl_2$ , 5 HEPES, 3 MgATP and 0.05 EGTA (KOH buffered). Solution 2 contained 15 Cs-glut, 10 CsCl, 10 NaCl, 1  $MgCl_2$ , 5 HEPES, 3 MgATP, 0.05 EGTA (CsOH buffered). All chemicals were from Sigma-Aldrich. Only recordings with an access resistance of less than 50 M $\Omega$  were used for analysis.

### 2.4. Identification of cell type by immunocytochemistry

In all recordings, cell identity ( $\alpha$ ,  $\beta$  or  $\delta$ ) was subsequently established by immunocytochemistry. Biocytin (0.5 mg ml<sup>-1</sup>) was included in the intracellular solution to allow identification of the cell recorded from. Following voltage-clamp experiments, islets were fixed with 4% formaldehyde in phosphate-buffered saline (PBS) overnight and permeabilized with 0.3% Triton X-100. Non-specific binding was blocked by pre-treatment for 2 h with 5% normal goat serum before incubating with the different primary antibodies for 4–12 h (guinea pig anti-insulin (Abcam, Cambridge, UK), sheep anti-glucagon (Sigma-Aldrich, St Louis, MO) and rabbit anti-somatostatin (Vector Labs, Burlingame, CA)). After washing with PBS, the islet was incubated for 1 h in secondary antibodies (Alexa 633 goat anti-guinea pig (insulin), Alexa 405 goat anti-mouse (glucagon) and Alexa 543 goat anti-rabbit (somatostatin)). Biocytin labelling was visualized by using Alexa Fluor 488 conjugated streptavidin (0.04 mg ml<sup>-1</sup>; Thermo Fisher). Islets were then washed and imaged on a confocal microscope (Axioskop 2 upright microscope fitted with a Zeiss LSM 510 meta confocal and a chameleon multiphoton module).

### 2.5. Electrophysiological variables

For every cell, several electrophysiological variables were recorded and characterized (table 1). All analyses were conducted blinded to cell type. The electrophysiological variables quantified are described in appendix A.

### 2.6. Multinomial logistic regression model for predicting islet cell type

A multinomial logistic regression model was constructed. For a given set of electrophysiological measures from a specific cell recording, this model can be used to predict the cell type. The model process requires a dataset for constructing (model construction dataset;  $N = 175$  cell recordings) and validating (model validation dataset;  $N = 113$  cell recordings) the model. A description of this model and the modelling process is given in appendix B.

**Table 1.** Variables quantified/characterized and used in the construction of the multinomial logistic regression model of islet cell type.

| variable ( $X_i$ )     | description  | continuous/categorical   |
|------------------------|--|--|
| animal strain          | strain of the animal from which cell recording taken   | categorical [1 = C57BL6; 2 = EPAC2-KO; 3 = Glu-; 4 = NMRI; 5 = SST-Cherry] |
| double sigmoid         | does the steady-state inactivation of $\text{Na}^+$ currents exhibit a double or single sigmoidal shape? | categorical [0 = single; 1 = double]                                       |
| $V_{zh}$               | half-inactivation of $\text{Na}^+$ current   | continuous   |
| $k_h$                  | slope factor of inactivation of $\text{Na}^+$ current  | continuous   |
| $R^2$                  | goodness-of-fit of the sigmoidal function to steady-state $\text{Na}^+$ current data                     | continuous   |
| $I_{\max}$             | maximum $\text{Na}^+$ current evoked   | continuous   |
| $I_{\max 70}$          | $\text{Na}^+$ current evoked from a holding potential of $-70$ mV  | continuous   |
| $C_{\text{cell}}$      | cell capacitance   | continuous   |
| $R_{\text{access}}$    | access (series) resistance of recording  | continuous   |
| tail current           | presence of a tail current in current–voltage data (see §3.5)  | categorical [0 = no; 1 = yes]  |
| transient current      | presence of a transient outward current (see §3.6)   | categorical [0 = no; 1 = yes]  |
| $I_{\text{leak}}$      | leak current of the recording  | continuous   |
| $R_{\text{input}}$     | input (seal) resistance of the recording in 1 mM glucose   | continuous   |
| ratio current          | ratio of $I_{\max}$ and $I_{\max 70}$  | continuous   |
| intracellular solution | solution 1 (K-glut) or solution 2 (Cs-glut)  | categorical [solution 1; solution 2]                                       |

The multinomial logistic regression model was constructed in SPSS (IBM, Armonk, NY). The model developed was coded into a freely available Matlab toolbox for predicting cell type. The toolbox and SPSS files are available from GitHub ([https://github.com/IsletCellType/IsletCellType\\_GitHub](https://github.com/IsletCellType/IsletCellType_GitHub)). The toolbox uses the multinomial logistic regression model presented to predict cell type, given a set of user-defined inputs (electrophysiological variables from the recorded cell). We have also made available on GitHub the entire dataset of 288 cell recordings that can be tested with the multinomial regression model.

## 2.7. Statistical tests of electrophysiological variables and analysis

All data are reported as mean  $\pm$  s.e.m., unless otherwise stated. SD refers to the standard deviation and  $N$  refers to the number of cell recordings. Statistical significance was defined as  $p < 0.05$ .

All recorded variables were compared across cell types using one-way ANOVA (PRISM5; GraphPad Software, San Diego, CA). If the data passed normality criteria (D'Agostino's test of normality and Bartlett's test of equal variances), a parametric test was conducted with the appropriate post hoc test (Tukey). If the normality criteria were not met, a Kruskal–Wallis test with Dunn's multiple comparison test was conducted.

Some of the variables used to identify cell type, such as the presence/absence of an outward transient current, are categorical (table 1). A contingency table analysis (Pearson's  $\chi^2$ ) will test whether there is an association between this variable and cell type. For post hoc tests, we adopted the approach described by Sharpe [57]; contingency tables were partitioned into  $2 \times 2$  tables, and a Fisher's exact test was conducted [57].

## 2.8. Conductance-based models

Conductance-based (Hodgkin–Huxley-like) models were used to simulate electrical activity in a model of an  $\alpha$ -cell and a  $\delta$ -cell. All conductance-based models were solved numerically

in the software package XPPAUT [58] using the variable step size method CVODE with absolute and relative tolerances of  $10^{-10}$ . The models are described in appendix C and can be obtained from GitHub (<https://github.com/IsletCellType>).

In what follows, it will be clear from the context whether we are referring to either (i) a conductance-based model of  $\alpha$ - or  $\delta$ -cell electrical activity or (ii) a multinomial logistic regression model for predicting islet cell type.

## 3. Results

We analysed the electrophysiological variables of 288 cells in intact islets from mice with a normoglycaemic phenotype.

### 3.1. Cell capacitance is an inadequate identifier of islet cell type

Cell capacitance ( $C_{\text{cell}}$ ) in  $\beta$ -cells ( $5.8 \pm 0.3$  pF,  $N = 56$ ) was significantly larger than that seen in  $\alpha$ -cells ( $4.2 \pm 0.1$  pF,  $N = 141$ ;  $p < 0.001$ ) and  $\delta$ -cells ( $4.3 \pm 0.1$  pF,  $N = 91$ ;  $p < 0.001$ ; figure 1*a*).  $\alpha$ -Cells and  $\delta$ -cells did not differ in their cell size ( $p = 0.556$ ). Given that  $C_{\text{cell}}$  is frequently used to identify cell type [13,34,36,39,40,42,44,49], we constructed a multinomial logistic regression model to investigate whether  $C_{\text{cell}}$  alone can identify cell type (equation (B 2) and table 2). The model identified  $\alpha$ -cells with 89% accuracy, but poorly identified  $\beta$ -cells (11/40 were identified correctly) and  $\delta$ -cells (1/62). Thus  $C_{\text{cell}}$  alone is an inadequate indicator of cell type.

### 3.2. $K_{\text{ATP}}$ conductance is largest in $\beta$ -cells

The whole-cell conductance ( $G$ ) was larger in  $\beta$ -cells ( $1.7 \pm 0.2$  nS,  $N = 56$ ) than in  $\alpha$ -cells ( $0.9 \pm 0.1$  nS,  $N = 141$ ;  $p < 0.001$ ) or  $\delta$ -cells ( $1.0 \pm 0.1$  nS,  $N = 91$ ;  $p = 0.005$ ; figure 1*b*). There was no difference in  $G$  between  $\alpha$ -cells and  $\delta$ -cells ( $p = 0.215$ ).

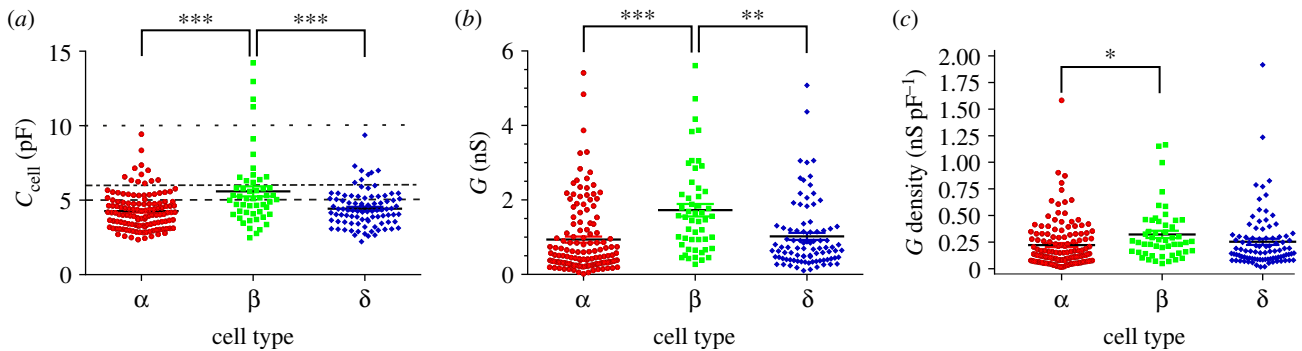


**Figure 1.** Differences in cell size and resting conductance between islet cell types. (a) Cell capacitance ( $C_{\text{cell}}$ ), (b) input conductance ( $G$ ) and (c) conductance density ( $G/C_{\text{cell}}$ ) in  $\alpha$ -cells ( $N = 141$ ),  $\beta$ -cells ( $N = 56$ ) and  $\delta$ -cells ( $N = 91$ ). Criteria for identifying cell type based on a cut-off for  $C_{\text{cell}}$ , such as  $>5$  pF (dashed; [42]) or  $>6$  pF (dashed-dotted; Andersson *et al.* [34] and Guo *et al.* [13]), are included. One-way ANOVA with Tukey's post hoc test (\*\* $p < 0.01$ ; \*\*\* $p < 0.001$ ). (Online version in colour.)

$G$  density ( $G$  normalized by  $C_{\text{cell}}$ ) in  $\alpha$ -cells ( $0.22 \pm 0.02$  nS pF $^{-1}$ ,  $N = 141$ ) was statistically lower than in  $\beta$ -cells ( $0.33 \pm 0.03$  nS pF $^{-1}$ ,  $N = 56$ ;  $p = 0.017$ ; figure 1c).  $G$  density in  $\delta$ -cells ( $0.25 \pm 0.03$  nS pF $^{-1}$ ,  $N = 91$ ) was no different from that in  $\beta$ -cells ( $p = 0.184$ ) or  $\alpha$ -cells ( $p = 0.536$ ).

### 3.3. Na $^{+}$ currents are largest in $\delta$ -cells (not $\alpha$ -cells)

The maximum amplitude of the Na $^{+}$  current ( $I_{\text{max}}$ ; figure 2a) evoked in  $\alpha$ -cells ( $-465 \pm 19$  pA,  $N = 141$ ) was significantly smaller than that in  $\beta$ -cells ( $-720 \pm 50$  pA,  $N = 56$ ;  $p < 0.001$ ) and  $\delta$ -cells ( $-846 \pm 37$  pA,  $N = 91$ ;  $p < 0.001$ ; figure 2b). There was no difference in  $I_{\text{max}}$  between  $\delta$ - and  $\beta$ -cells ( $p = 0.14$ ). We explored whether  $I_{\text{max}}$  could be used to predict cell type in a multinomial logistic regression model (equation (B 2) and table 2), given that it is frequently used to identify cell type [29,35,39,40,45–47]. The model identified cell type with 57.7% accuracy, and failed to identify any  $\beta$ -cells. Therefore,  $I_{\text{max}}$  alone cannot reliably identify cell type.

### 3.4. $V_{2h}$ cannot reliably distinguish $\beta$ -cells from non- $\beta$ -cells

The voltage dependence of steady-state inactivation of the Na $^{+}$  current differed between cell types (figure 2c–e). Inactivation in  $\alpha$ -cells was half-maximal ( $V_{2h}$ ) at  $-38.4 \pm 1.4$  mV ( $N = 141$ ), as observed in pancreatic slices [40]. This value was not statistically different from that in  $\delta$ -cells ( $-41.4 \pm 1.8$  mV,  $N = 91$ ;  $p = 0.187$ ). In contrast,  $V_{2h}$  was significantly more hyperpolarized in  $\beta$ -cells ( $-78.3 \pm 3$  mV,  $N = 56$ ) than in either  $\alpha$ -cells ( $p < 0.001$ ) or  $\delta$ -cells ( $p < 0.001$ ). There was no difference in  $V_{2h}$  between  $\alpha$ - and  $\delta$ -cells ( $p = 0.22$ ).

As it is more hyperpolarized in  $\beta$ -cells,  $V_{2h}$  is often used to distinguish  $\beta$ -cells from non- $\beta$ -cells [11,29,39–41,44–47,49,50]. We therefore explored whether  $V_{2h}$  alone could be used to distinguish cell type. We first did this by investigating whether a simple criterion could enrich the  $\beta$ -cell population; the number of cells with  $V_{2h} < a$  fixed cut-off were counted. The cut-off ranged from  $-25$  to  $-100$  mV in 1 mV increments. For each cut-off, the numbers of  $\alpha$ -,  $\beta$ - and  $\delta$ -cells that pass this criterion were counted. The percentage of these cells that were  $\beta$ -cells ( $\beta$ -cell enrichment; figure 2f) and the percentage of  $\beta$ -cells that pass this criterion (figure 2g) were then calculated. As the cut-off became more hyperpolarized,  $\beta$ -cell enrichment increased. However, the percentage of  $\beta$ -cells that passed this criterion also decreased. Therefore, attempting to enrich  $\beta$ -cells with a criterion based on  $V_{2h}$  comes with a cost—a drastic

decrease in sample size. We further demonstrated that  $V_{2h}$  cannot reliably identify cell type by constructing a multinomial logistic regression model of cell type, with one independent variable ( $V_{2h}$ ; equation (B 2)). The model was unable to identify  $\delta$ -cells (0% correct) and correctly identified cell type with an overall accuracy of 54% only (table 2).

The slope factor of steady-state inactivation was greater in  $\beta$ -cells ( $k_h = -13.1 \pm 0.8$  mV,  $N = 56$ ) than in  $\alpha$ -cells ( $k_h = -9.5 \pm 0.4$  mV,  $N = 141$ ;  $p = 0.001$ ) and  $\delta$ -cells ( $k_h = -7.7 \pm 0.3$  mV,  $N = 91$ ;  $p < 0.001$ ; figure 2e). The slope factor was also significantly smaller in  $\alpha$ -cells than in  $\delta$ -cells ( $p < 0.001$ ).

### 3.5. Ca $^{2+}$ tail currents are most prominent in $\delta$ -cells

We next analysed slow tail currents in all cells (figure 3a,b). The average time constant of decay in  $\delta$ -cells ( $1.9 \pm 0.2$  ms;  $N = 91$ ) was significantly greater than that in  $\alpha$ -cells ( $0.58 \pm 0.03$ ,  $N = 141$ ;  $p < 0.001$ ) and  $\beta$ -cells ( $0.54 \pm 0.04$ ,  $N = 56$ ;  $p < 0.001$ ). Slow tail currents were present in 0/141  $\alpha$ -cells, 4/56 (7%)  $\beta$ -cells and 59/91 (65%)  $\delta$ -cells (figure 3c). The presence of a slow tail current in  $\delta$ -cells was statistically different from that in  $\alpha$ -cells ( $p < 0.001$ ) and  $\beta$ -cells ( $p < 0.001$ ). This contrasts with previous studies which have used the presence of a slow tail current to identify  $\alpha$ -cells [29,31,38,46].

### 3.6. The presence of a transient outward current is not unique to $\alpha$ -cells

Many groups have used the presence of a transient TEA-resistant outward current (putatively an A-type K $^{+}$  current) to define an  $\alpha$ -cell [29,31,38,46–48]. We therefore characterized the presence of this current in all recordings (figure 4). Transient outward currents were seen in 14/141 (10%)  $\alpha$ -cells, 0/56 (0%)  $\beta$ -cells and 23/91 (25%)  $\delta$ -cells (figure 4b). The presence of a transient outward current was statistically different between  $\delta$ -cells and  $\alpha$ -cells ( $p = 0.0029$ ). When only recordings with intracellular solution 1 (K-glut) were considered, its prevalence in  $\delta$ -cells (67%) was also greater than that in  $\alpha$ -cells (20%;  $p = 0.0001$ ; figure 4b).

### 3.7. A binary logistic regression model for identifying $\beta$ -cells versus non- $\beta$ -cells

Electrophysiological criteria have been employed in many studies to distinguish  $\beta$ -cells from non- $\beta$ -cells. For example, islet cells with  $C_{\text{cell}} > 5$  pF [42] and  $C_{\text{cell}} > 6$  pF [13] have been considered to be  $\beta$ -cells. We therefore investigated whether a

**Table 2.** Single electrophysiological variables inadequately identify islet cell type. For each electrophysiological variable, a multinomial logistic regression model (equation (B 2)) was constructed to investigate how accurately this variable can identify cell type on its own. Each row represents a separate model, constructed with one independent variable ( $X_i$ ). The parameter estimates are relative to the  $\delta$ -cell reference category. For variable descriptions, see table 1. All models were constructed using the sample values from the model construction dataset ( $N = 175$  cells).

| variable ( $X_i$ )  | $B_{0\alpha}$     |        |                                 | $B_{0\beta}$ |                   |        | $B_{1\beta}$                   |        |              | observed/predicted [% correct] |              |         |
|---------------------|-------------------|--------|---------------------------------|--------------|-------------------|--------|--------------------------------|--------|--------------|--------------------------------|--------------|---------|
|                     | mean $\pm$ s.e.m. | sig.   | mean $\pm$ s.e.m.               | sig.         | mean $\pm$ s.e.m. | sig.   | mean $\pm$ s.e.m.              | sig.   | $\alpha$     | $\beta$                        | $\delta$     | overall |
| $C_{\text{cell}}$   | 0.78 $\pm$ 0.31   | 0.283  | -0.12 $\pm$ 0.14                | 0.40         | -2.58 $\pm$ 0.70  | 0.00   | 0.42 $\pm$ 0.13                | 0.002  | 65/73 [89.0] | 11/40 [15.2]                   | 1/62 [6.9]   | 44.0    |
| $R_{\text{input}}$  | -0.01 $\pm$ 0.26  | 0.97   | 7.8 $\pm$ 9.3 $\times 10^{-5}$  | 0.40         | 0.72 $\pm$ 0.34   | 0.03   | 8.9 $\pm$ 2.5 $\times 10^{-4}$ | 0.00   | 53/73 [72.6] | 23/40 [57.5]                   | 0/62 [0]     | 43.4    |
| $I_{\text{max}}$    | 2.34 $\pm$ 0.45   | <0.001 | 3.4 $\pm$ 0.6 $\times 10^{-3}$  | <0.001       | -0.37 $\pm$ 0.49  | 0.45   | 1.1 $\pm$ 0.6 $\times 10^{-3}$ | 0.07   | 60/73 [82.2] | 0/40 [0]                       | 41/62 [66.1] | 57.7    |
| $V_{2h}$            | 0.49 $\pm$ 0.42   | 0.27   | 8.0 $\pm$ 0.01 $\times 10^{-3}$ | 0.39         | -3.89 $\pm$ 0.67  | <0.001 | -0.06 $\pm$ 0.01               | <0.001 | 64/73 [87.7] | 31/40 [77.5]                   | 0/62 [0]     | 54.3    |
| $k_h$               | -0.89 $\pm$ 0.42  | 0.052  | 0.12 $\pm$ 0.05                 | 0.016        | -2.6 $\pm$ 0.56   | <0.001 | 0.22 $\pm$ 0.05                | <0.001 | 42/73 [57.5] | 8/40 [20]                      | 36/62 [58.1] | 49.1    |
| $I_{\text{leak}}$   | 0.70 $\pm$ 0.26   | <0.001 | 0.04 $\pm$ 0.01                 | 0.007        | -0.39 $\pm$ 0.28  | 0.17   | 0.002 $\pm$ 0.01               | 0.80   | 61/73 [83.6] | 0/40 [0]                       | 23/62 [37.1] | 48.0    |
| $R_{\text{access}}$ | 0.1 $\pm$ 0.5     | 0.83   | 2.5 $\pm$ 2 $\times 10^{-3}$    | 0.90         | -0.55 $\pm$ 0.55  | 0.34   | 5.0 $\pm$ 2.3 $\times 10^{-3}$ | 0.83   | 73/73 [100]  | 0/40 [0]                       | 0/62 [0]     | 41.7    |
| double sigmoid      | 0.20 $\pm$ 0.45   | 0.65   | -0.04 $\pm$ 0.49                | 0.93         | 1.3 $\pm$ 0.38    | <0.001 | -3.16 $\pm$ 0.54               | <0.001 | 62/73 [84.9] | 32/40 [80]                     | 0/62 [0]     | 53.7    |
| tail current        | -18.8 $\pm$ 0.24  | <0.001 | 20.02 $\pm$ 0.01                | <0.001       | -19.4 $\pm$ 0.27  | <0.001 | 20.02 $\pm$ 0.01               | <0.001 | 73/73 [100]  | 0/40 [0]                       | 40/62 [64.5] | 64.6    |
| transient current   | -0.55 $\pm$ 0.38  | 0.15   | 0.91 $\pm$ 0.42                 | 0.03         | -18.3 $\pm$ 0.22  | <0.001 | 18.2 $\pm$ 0.01                | <0.001 | 62/73 [84.9] | 0/40 [0]                       | 19/62 [30.6] | 47.3    |

simple rule based on  $C_{\text{cell}}$  could distinguish  $\beta$ -cells from non- $\beta$ -cells. The number of cells with  $C_{\text{cell}} >$  a fixed cut-off (4–10 pF in 0.2 pF increments) were counted. The percentage of cells that passed the criterion that were  $\beta$ -cells ( $\beta$ -cell enrichment; figure 5a) and the percentage of all  $\beta$ -cells that pass this criterion (figure 5b) were then calculated. For example, 41 cells passed the criterion  $C_{\text{cell}} >$  6 pF; 12  $\alpha$ -cells, 21  $\beta$ -cells and eight  $\delta$ -cells. Therefore, this rule only enriched  $\beta$ -cells in the sample to 51%. Moreover, 35 (56–21)  $\beta$ -cells did not pass this criterion; a 63% reduction in potential sample size. The results were still poor when we applied a stricter criterion; only four  $\beta$ -cells passed the criterion  $C_{\text{cell}} >$  9.4 pF (100% enrichment), but this came with a 92% reduction in sample size (4/56  $\beta$ -cells). We conclude that using  $C_{\text{cell}}$  alone to distinguish  $\beta$ -cells from non- $\beta$ -cells is inadequate.

We therefore used the model construction dataset to construct a binary logistic regression model, to determine whether the electrophysiological variables could collectively distinguish  $\beta$ -cells from non- $\beta$ -cells (figure 5c–f). The electrophysiological variables significantly predicting cell type ( $\beta$ -cells from non- $\beta$ -cells) included  $C_{\text{cell}}$  and  $I_{\text{max}}$ . The model was able to distinguish  $\beta$ -cells from non- $\beta$ -cells with 91% accuracy in the model construction dataset; 32/40  $\beta$ -cells were correctly assigned as  $\beta$ -cells, and 127/135 non- $\beta$ -cells were assigned as non- $\beta$ -cells (figure 5c,d). When the model was applied to the model validation dataset it again could identify  $\beta$ -cells from non- $\beta$ -cells with 97% accuracy (figure 5e,f). We conclude that, when taken together, the electrophysiological variables quantified can distinguish  $\beta$ -cells from non- $\beta$ -cells with a high degree of accuracy.

### 3.8. A multinomial logistic regression model for identifying cell type

A multinomial logistic regression model was developed to investigate whether the electrophysiological variables could be used together to identify all three cell types, rather than just distinguish  $\beta$ -cells from non- $\beta$ -cells. The model construction dataset was used for fitting the model parameters (table 3). The modelling process (see appendix B) yielded a final model based on 10 electrophysiological variables (figure 6 and table 4). Importantly, potential confounders, such as animal strain and intracellular solution, did not significantly increase the maximum likelihood of observing the sample values. The model was stable; both forward-entry and backward-elimination methods of variable selection produced a model with similar variables and parameter estimates (figure 6a and table 4). The final model constructed with the forward-entry method included the electrophysiological variables  $I_{\text{leak}}$ ,  $R_{\text{access}}$ ,  $C_{\text{cell}}$ ,  $k_{\text{lv}}$ ,  $I_{\text{max}}$ ,  $R_{\text{input}}$ , transient current, ratio current,  $V_{2h}$  and tail current. In what follows, this model is used to predict islet cell type.

The model was applied to the model validation dataset ( $N = 113$ ; table 3) to see how well it can identify cell type. The model identified  $\alpha$ -cells with 94% accuracy,  $\delta$ -cells with 90% accuracy and  $\beta$ -cells with 100% accuracy (figure 6b,c). These data demonstrate that the model is applicable to other datasets, as it can predict islet cell type in the model validation dataset with an overall accuracy of 94%.

To rank the variables in the model by their importance for identifying islet cell type, standardized coefficients were calculated as described by Menard [60].  $V_{2h}$  and  $C_{\text{cell}}$ —variables typically used to distinguish  $\beta$ -cells from non- $\beta$ -cells

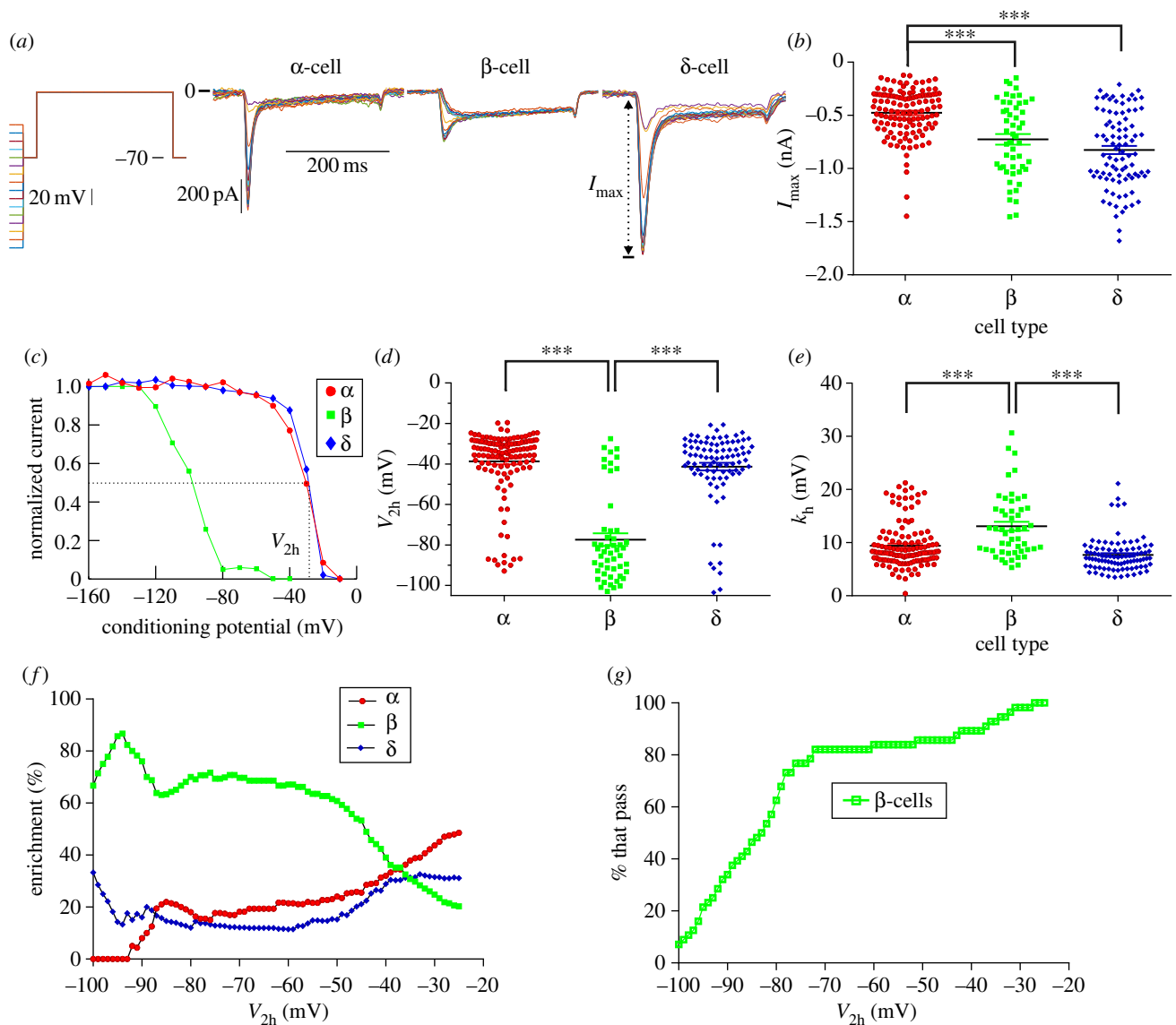


**Figure 2.** Na<sup>+</sup> currents are smallest in  $\alpha$ -cells. The maximum Na<sup>+</sup> current evoked (a,  $I_{max}$ ) by a 200 ms test pulse to 0 mV, following preconditioning pulses, was measured in all cells (b). These data were also used to calculate the normalized peak current as a function of the conditioning potential (c). For each cell, these data were fitted with a sigmoid to quantify the half-inactivation  $V_{2h}$  (d) and the slope factor  $k_h$  (e). The number of cells with  $V_{2h} < -25$  to  $-100$  mV was counted. The percentage of these cells that are  $\beta$ -cells (enrichment, f) and the percentage of all  $\beta$ -cells that pass this criterion (% that pass, g) were then calculated. One-way ANOVA with Tukey's post hoc test ( $***p < 0.001$ ).  $N = 141$   $\alpha$ -cells,  $N = 56$   $\beta$ -cells and  $N = 91$   $\delta$ -cells. (Online version in colour.)

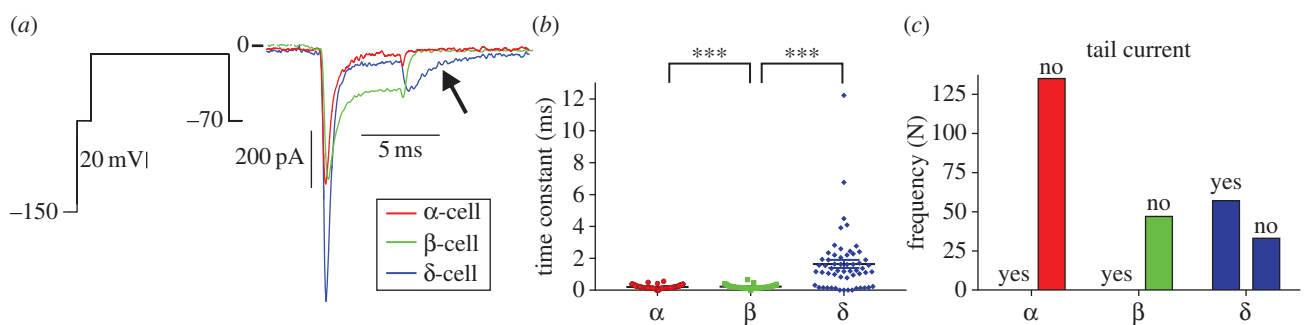


**Figure 3.** The presence of a slow Ca<sup>2+</sup> tail current is a feature of  $\delta$ -cells (not  $\alpha$ -cells). (a) The presence of a slow tail current was characterized in each of the 288 cell recordings. (b) Following a test pulse to 30 mV, a slow tail current was present on the decay to  $-70$  mV if the time constant of decay of the tail current was  $>1.5$  ms. (c) The slow tail current was most prevalent in  $\delta$ -cells. One-way ANOVA with Tukey's post hoc test ( $***p < 0.001$ ).  $N = 141$   $\alpha$ -cells,  $N = 56$   $\beta$ -cells and  $N = 91$   $\delta$ -cells. (Online version in colour.)

[3,11,29,35,37–41,44–47,50]—ranked low (eighth and 12th, respectively) on the list (figure 6e(i)). The most important variable for distinguishing  $\delta$ -cells from  $\alpha$ -cells was the presence of a slow Ca<sup>2+</sup> tail current (figure 6e(ii)). The presence of an A-current—which has frequently been employed to

distinguish these two cell types [29,31,38,46–48]—was not the highest ranking variable. The variable that ranked second was  $I_{max}$ , indicating that a large Na<sup>+</sup> current is an important distinguishing feature of  $\delta$ -cells from  $\alpha$ -cells. These findings do not conform to standard practice for identifying

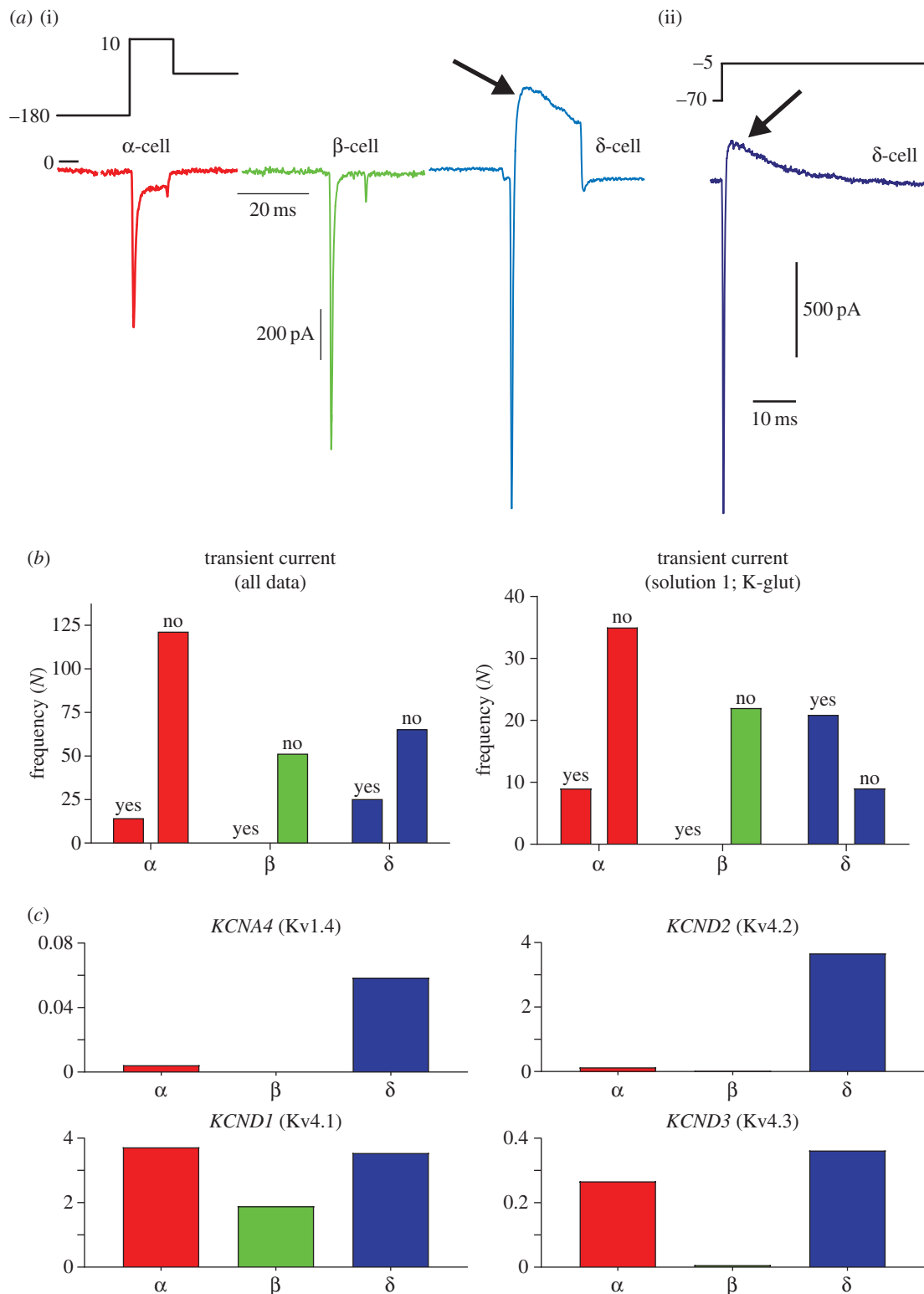


**Figure 4.** The A-type channel is expressed in both  $\alpha$ - and  $\delta$ -cells. (a) The presence of a transient outward current (arrow) was characterized in each of the 288 cell recordings. (b) The presence of a transient outward current (A-type) was not a feature unique to  $\alpha$ -cells; it was actually most prevalent in  $\delta$ -cells.  $N = 288$  recordings. (c) For each cell type, we represented the number of cells that did (yes) and did not (no) exhibit A-type currents in recordings made in intracellular solution 1 (K-glut) only.  $N = 93$  recordings. (d) The genes encoding TEA-resistant Kv channels of A-type (fast inactivating) are differentially expressed in both  $\alpha$ -cells and  $\delta$ -cells. Transcriptome data from DiGruccio *et al.* [59], reproduced with permission. (Online version in colour.)

cell type and therefore highlight the importance of using our multinomial logistic regression model to identify cell type.

### 3.9. Incorrectly identified $\alpha$ -cells have $\beta$ -cell-like characteristics

We characterized the cells whose cell type was incorrectly identified by the model (figure 7). The model incorrectly

identified 14/141  $\alpha$ -cells. In those  $\alpha$ -cells incorrectly assigned (as  $\beta$ - or  $\delta$ -cells), the measured  $V_{2h}$  was significantly hyperpolarized ( $-64.1 \pm 7.1$ ) compared with correctly assigned  $\alpha$ -cells ( $-35.3 \pm 1.1$ ;  $p = 0.01$ ). Moreover, it did not differ from that of  $\beta$ -cells that were correctly identified by the model ( $-81.8 \pm 2.8$ ;  $p = 0.42$ ; figure 7a(i)). Furthermore, 64% of the incorrectly identified  $\alpha$ -cells (9/14) exhibited a double sigmoidal  $h_{\infty}$ ,

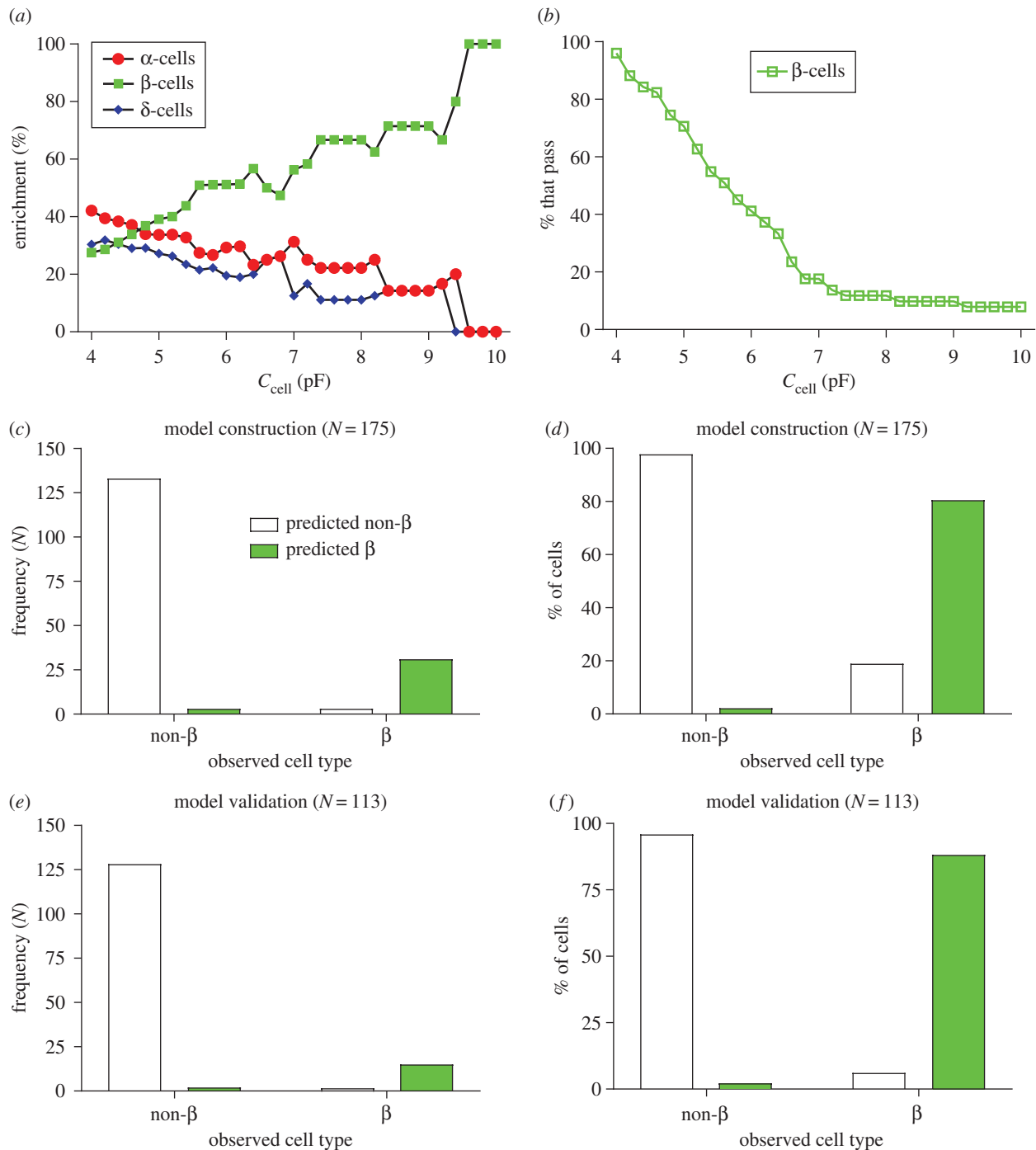


**Figure 5.** A binary logistic regression model is able to reliably distinguish  $\beta$ - from non- $\beta$ -cells. We attempted to distinguish  $\beta$ -cells from non- $\beta$ -cells using a simple criterion. We considered  $\beta$ -cells as having a  $C_{\text{cell}} >$  a fixed cut-off (4–10 pF in 0.2 pF increments; see dashed lines in figure 1a). We calculated, for this cut-off, (a) the percentage of cells that pass this criterion that are  $\beta$ -cells ( $\beta$ -cell enrichment) and (b) the percentage of  $\beta$ -cells from the total  $\beta$ -cell population that pass this criterion (% that pass). Increasing the cut-off to 9.4 pF enriched the  $\beta$ -cell population to 100%, but significantly reduced the number of  $\beta$ -cells passing the criterion (to 4/56 cells (7%)). (c,d) A binary logistic regression model for distinguishing  $\beta$ - from non- $\beta$ -cells. The model could accurately distinguish cells in the model construction dataset. 97.8% of non- $\beta$ -cells were assigned as non- $\beta$ -cells by the model, and 91.2% of  $\beta$ -cells were assigned as  $\beta$ -cells by the model. (e,f) The model could also accurately distinguish  $\beta$ -cells from non- $\beta$ -cells in the model validation dataset. (Online version in colour.)

compared with 2.5% of cells in the correctly labelled  $\alpha$ -cell population (figure 7a(ii)). These incorrectly identified  $\alpha$ -cells therefore have ‘ $\beta$ -cell-like’  $\text{Na}^+$  channel properties. The model supported this idea; the probability that the incorrectly identified  $\alpha$ -cells were  $\beta$ -cells ( $P_{\beta} = 0.52 \pm 0.1$ ) was significantly larger than for correctly identified  $\alpha$ -cells ( $P_{\beta} = 0.05 \pm 0.01$ ;  $p = 0.001$ ; figure 7b). In particular, the model revealed that these  $\alpha$ -cells have ‘ $\beta$ -cell-like’ properties.

### 3.10. The model can identify islet cell type in mice with a hyperglycaemic phenotype

To investigate whether the model could accurately identify islet cell type from mice with a hyperglycaemic phenotype, an additional 13 cell recordings were made in  $\beta\text{V59M}$  mice and 15 in wild-type control mice (WT; figure 8). The model identified cell type in recordings from WT islets with 100% accuracy, identifying all five  $\beta$ -cells ( $P_{\beta} = 0.95 \pm 0.04$ ) and 10  $\alpha$ -cells

**Table 3.** Datasets used for model construction and model validation. One-way ANOVA with Kruskal–Wallis post hoc tests;  $p[\alpha$  versus  $\beta]$ ,  $p[\alpha$  versus  $\delta]$ ,  $p[\beta$  versus  $\delta]$ . For categorical variables, the count frequency in each category (Y/N = yes/no) is reported and the post hoc  $p$ -values are computed as described in Sharpe [57]. Transient current:  $[N]$  = number of recordings in intracellular solution 1 ( $K^+$ –Glut solution). See table 1 for variable descriptions.

| variables ( $X_i$ )               | $\alpha$ -cells |        |     |  | $\beta$ -cells |        |     |  | $\delta$ -cells |        |     |  |
|-----------------------------------|-----------------|--------|-----|--|----------------|--------|-----|--|-----------------|--------|-----|--|
|                                   | mean            | s.e.m. | $N$ |  | mean           | s.e.m. | $N$ |  | mean            | s.e.m. | $N$ |  |
| model construction dataset        |                 |        |     |  |                |        |     |  |                 |        |     |  |
| $I_{\text{leak}}$ (pA)            | −12.1           | 1.5    | 73  |  | −19.3          | 3.0    | 40  |  | −20.4           | 2.6    | 62  |  |
| $R_{\text{input}}$ (G $\Omega$ )  | 2.2             | 0.2    | 73  |  | 0.9            | 0.1    | 40  |  | 1.9             | 0.2    | 62  |  |
| $C_{\text{cell}}$ (pF)            | 4.3             | 0.2    | 73  |  | 6.0            | 0.4    | 40  |  | 4.5             | 0.2    | 62  |  |
| $R_{\text{access}}$ (M $\Omega$ ) | 22.7            | 0.9    | 73  |  | 22.9           | 1.4    | 40  |  | 22.6            | 1.2    | 62  |  |
| $K_h$ (mV)                        | 9.6             | 0.5    | 73  |  | 12.6           | 1.0    | 40  |  | 7.9             | 0.5    | 62  |  |
| $I_{\text{max}}$ (pA)             | −492            | 29     | 73  |  | −702           | 59     | 40  |  | −831            | 44     | 62  |  |
| $V_{2h}$ (mV)                     | −39.7           | 2.1    | 73  |  | −78.0          | 3.7    | 40  |  | −42.4           | 2.4    | 62  |  |
| tail current (yes)                | 0               |        | 73  |  | 0              |        | 40  |  | 40/62           |        | 62  |  |
| transient current (yes)           | 11 [24]         |        | 73  |  | 0 [15]         |        | 40  |  | 16 [16]         |        | 62  |  |
| double sigmoid (yes)              | 11              |        | 73  |  | 32             |        | 40  |  | 9               |        | 62  |  |
| model validation dataset          |                 |        |     |  |                |        |     |  |                 |        |     |  |
| $I_{\text{leak}}$ (pA)            | −11.4           | 1.8    | 68  |  | −115           | 3.1    | 16  |  | −22.9           | 3.5    | 29  |  |
| $R_{\text{input}}$ (G $\Omega$ )  | 3.1             | 0.5    | 68  |  | 1.1            | 0.2    | 16  |  | 1.6             | 0.3    | 29  |  |
| $C_{\text{cell}}$ (pF)            | 4.5             | 0.1    | 68  |  | 5.3            | 0.3    | 16  |  | 4.3             | 0.2    | 29  |  |
| $R_{\text{access}}$ (M $\Omega$ ) | 21.8            | 0.9    | 68  |  | 23.9           | 2.0    | 16  |  | 26.5            | 1.5    | 29  |  |
| $K_h$ (mV)                        | 9.3             | 0.5    | 68  |  | 14.8           | 1.4    | 16  |  | 7.2             | 0.3    | 29  |  |
| $I_{\text{max}}$ (pA)             | −432            | 22     | 68  |  | −783           | 86     | 16  |  | −876            | 68     | 29  |  |
| $V_{2h}$ (mV)                     | −36.9           | 1.9    | 68  |  | −79.5          | 3.5    | 16  |  | −39.2           | 2.6    | 29  |  |
| tail current (yes)                | 0               |        | 68  |  | 0              |        | 16  |  | 19              |        | 29  |  |
| transient current (yes)           | 3 [21]          |        | 68  |  | 0 [7]          |        | 16  |  | 7 [11]          |        | 29  |  |
| double sigmoid (yes)              | 6               |        | 68  |  | 9              |        | 16  |  | 0               |        | 29  |  |

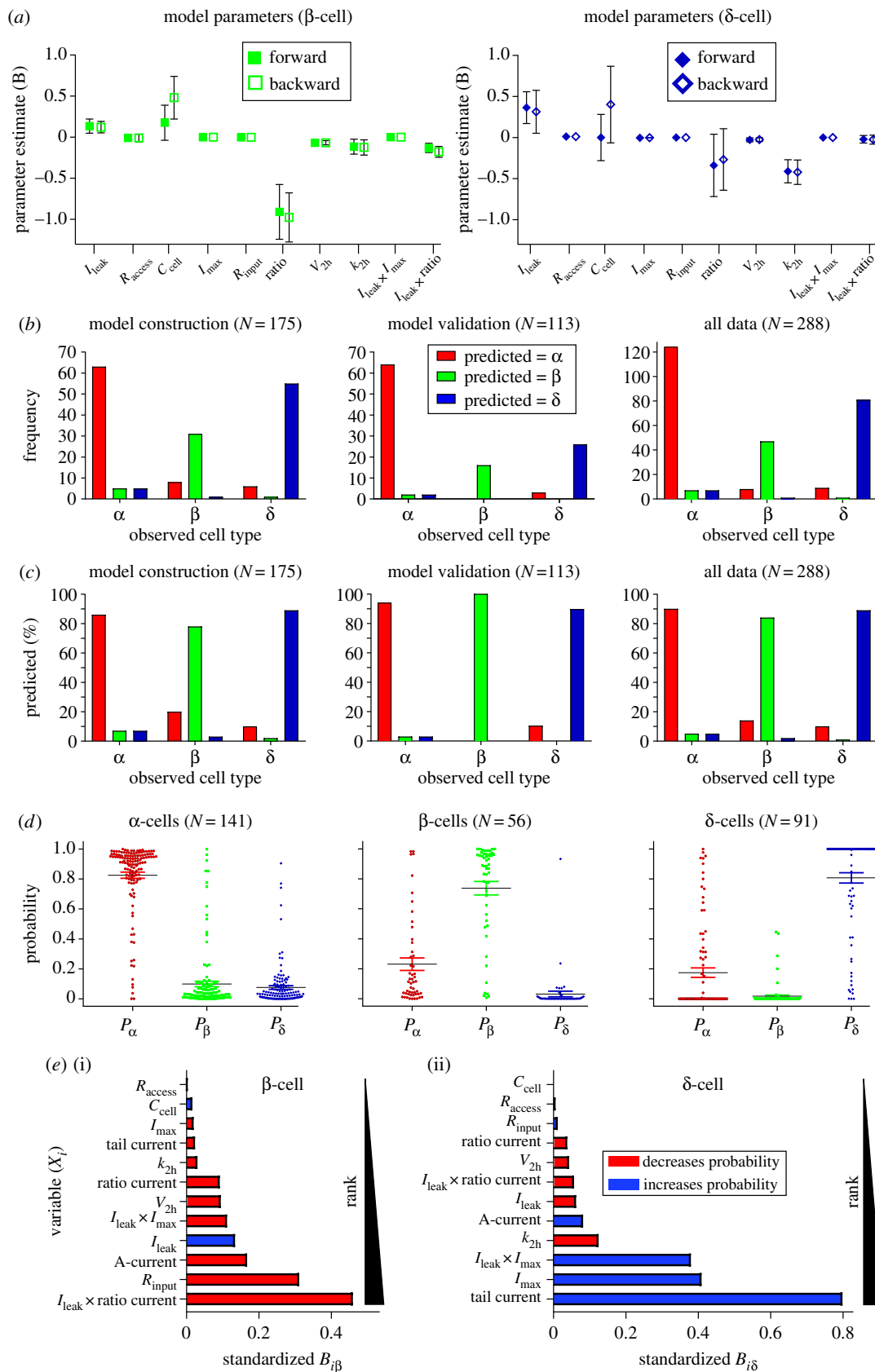


**Figure 6.** A multinomial logistic regression model is able to reliably identify islet cell type. A multinomial logistic regression model was constructed using the model construction dataset ( $N = 175$  cell recordings). (a) The forward-entry and backward-elimination methods of variable selection resulted in a final model with similar parameter values. (b) The forward-entry model was used to predict islet cell type in the model construction, model validation and entire dataset. Bar chart of observed (by immunocytochemistry) cell type by cell type predicted by the model. (c) Percentage of cells correctly identified by the model, for each cell type, in each dataset.  $N =$  frequency (cell count). (d) For all 288 cells, the probability (according to the model) that the cell is an  $\alpha$ - ( $P_{\alpha}$ ),  $\beta$ - ( $P_{\beta}$ ) and  $\delta$ -cell ( $P_{\delta}$ ) was calculated. The maximum of these was used to determine the cell type as identified by the model. (e) Standardized model coefficients. The coefficients from the model (equation (B 1), appendix B) were standardized by the method described by Menard [60], so that their importance for determining cell type could be ranked. (e(i)) Standardized model coefficients were calculated for the  $\beta$ -cell parameters  $B_{i\beta}$  (table 4, equation (B 1)). A red (blue, respectively) colour indicates that a SD increase in this variable decreases (increases) the probability that the cell type is  $\beta$ -cell (versus  $\alpha$ -cell). (e(ii)) A similar ranking was conducted for the variables and  $\delta$ -cell prediction. (Online version in colour.)

**Table 4.** Parameter estimates for a multinomial logistic regression model for predicting islet cell type. A multinomial logistic regression model of islet cell type, as written in equation (B 1), was constructed using the model construction dataset ( $N = 175$  cells). Both forward-entry and backward-elimination approaches were taken to determine which variables to include in the model ( $X_i$ ) and their associated parameter values ( $B_{\text{cell}}$ ,  $B_{\text{is}}$ ). The parameter estimates are relative to the  $\alpha$ -cell reference category. For variable descriptions, see table 1.

|                          | forward entry                                 |                       |                      |        | backward elimination  |                      |        |  |
|--------------------------|---|-----------------------|----------------------|--------|-----------------------|----------------------|--------|--|
|                          | variable ( $X_i$ )                            | $B_{i\beta}$          | s.e.m.               | sig.   | $B_{i\beta}$          | s.e.m.               | sig.   |  |
| $\beta$ -cell variables  | intercept                                     | -23.1                 | 2.2                  | <0.001 | -31.6                 | 4400                 | 0.99   |  |
|                          | $I_{\text{leak}}$                             | 0.13                  | 0.09                 | 0.12   | 0.122                 | 0.07                 | 0.081  |  |
|                          | $R_{\text{access}}$                           | $-8.8 \times 10^{-3}$ | $43 \times 10^{-3}$  | 0.84   | $10 \times 10^{-3}$   | $47 \times 10^{-3}$  | 0.824  |  |
|                          | $C_{\text{cell}}$                             | 0.18                  | 0.21                 | 0.41   | 0.48                  | 0.26                 | 0.064  |  |
|                          | $I_{\text{max}}$                              | $-10 \times 10^{-3}$  | $17 \times 10^{-3}$  | 0.553  | 0                     | 0.002                | 0.97   |  |
|                          | $R_{\text{input}}$                            | $-7.4 \times 10^{-4}$ | $3.6 \times 10^{-4}$ | 0.04   | $-1 \times 10^{-3}$   | 0                    | 0.022  |  |
|                          | ratio current                                 | -0.91                 | 0.63                 | 0.151  | -0.98                 | 0.69                 | 0.16   |  |
|                          | transient current (Y/N)                       | 22.4                  | 0                    | <0.001 | 24.9                  | 0                    | <0.001 |  |
|                          | $V_{2h}$                                      | $-6.8 \times 10^{-2}$ | $2.7 \times 10^{-2}$ | 0.009  | $-6.8 \times 10^{-2}$ | $2.6 \times 10^{-2}$ | 0.009  |  |
|                          | tail current (Y/N)                            | -0.99                 | 0                    | 0.99   | 4.53                  | 4400                 | 0.99   |  |
|                          | $k_{2h}$                                      | -0.11                 | 0.09                 | 0.21   | -0.13                 | 0.09                 | 0.18   |  |
|                          | $I_{\text{leak}} \times I_{\text{max}}$       | $-11 \times 10^{-6}$  | $13 \times 10^{-6}$  | 0.39   | $-22 \times 10^{-6}$  | $14 \times 10^{-5}$  | 0.87   |  |
|                          | $I_{\text{leak}} \times \text{ratio current}$ | -0.13                 | 0.06                 | 0.02   | -0.18                 | 0.07                 | 0.007  |  |
| $\delta$ -cell variables | variable ( $X_i$ )                            | $B_{i\delta}$         | s.e.m.               | sig.   | $B_{i\delta}$         | s.e.m.               | sig.   |  |
|                          | intercept                                     | 31.9                  | 2535                 | 0.990  | 31.4                  | 3137                 | 0.992  |  |
|                          | $I_{\text{leak}}$                             | 0.37                  | 0.194                | 0.060  | 0.314                 | 0.261                | 0.229  |  |
|                          | $R_{\text{access}}$                           | 0.012                 | 0.043                | 0.784  | 0.011                 | 0.045                | 0.803  |  |
|                          | $C_{\text{cell}}$                             | 0.001                 | 0.282                | 0.996  | 0.402                 | 0.467                | 0.390  |  |
|                          | $I_{\text{max}}$                              | -0.003                | 0.002                | 0.111  | -0.002                | 0.002                | 0.342  |  |
|                          | $R_{\text{input}}$                            | 0.000                 | 0.000                | 0.443  | 0.000                 | 0.000                | 0.439  |  |
|                          | ratio current                                 | -0.34                 | 0.38                 | 0.373  | -0.267                | 0.375                | 0.475  |  |
|                          | transient current (Y/N)                       | -3.6                  | 0.92                 | 0.000  | -3.713                | 0.981                | 0.000  |  |
|                          | $V_{2h}$                                      | -0.028                | 0.024                | 0.239  | -0.025                | 0.023                | 0.279  |  |
|                          | tail current (Y/N)                            | -29.6                 | 2535                 | 0.991  | -30.1                 | 3137                 | 0.992  |  |
|                          | $k_{2h}$                                      | -0.411                | 0.14                 | 0.004  | -0.422                | 0.15                 | 0.005  |  |
|                          | $I_{\text{leak}} \times I_{\text{max}}$       | 0.000                 | 0.000                | 0.069  | 0.000                 | 0.000                | 0.056  |  |
|                          | $I_{\text{leak}} \times \text{ratio current}$ | -0.021                | 0.05                 | 0.64   | -0.025                | 0.055                | 0.641  |  |

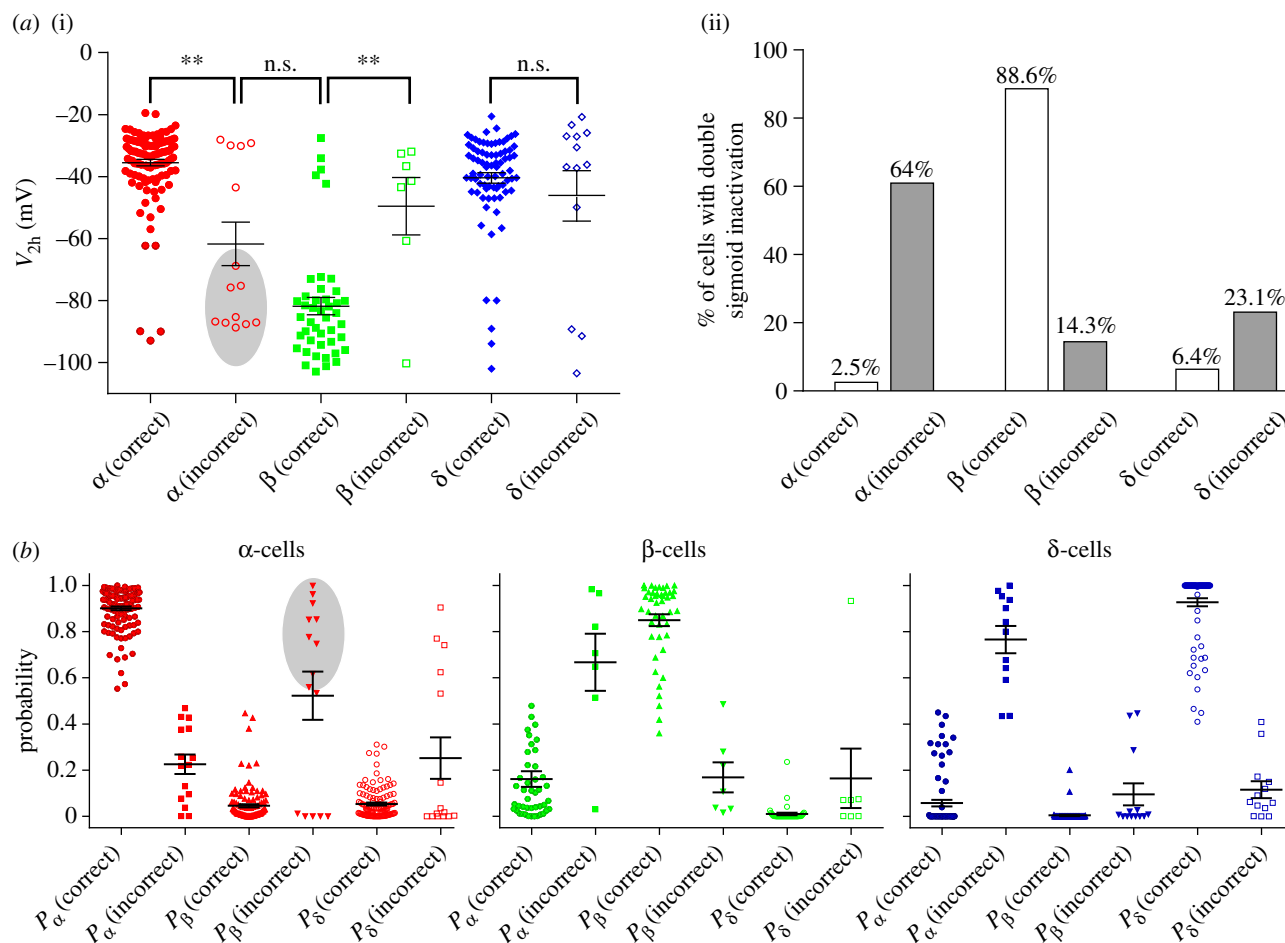


**Figure 7.** Properties of cells incorrectly identified by the multinomial logistic regression model. Cells were divided into those correctly and incorrectly identified by the model. (a(i))  $\alpha$ -cells that were incorrectly identified had a significantly hyperpolarized  $V_{2h}$  compared with  $\alpha$ -cells that were correctly predicted by the model. Furthermore, the incorrectly identified  $\alpha$ -cells had a  $V_{2h}$  that did not differ from (correctly identified)  $\beta$ -cells. (a(ii)) The proportion of cells exhibiting a double sigmoid was different across cells correctly and incorrectly identified by the model. (b) Model probabilities for each cell type, split by those correctly and incorrectly identified by the model. The shaded region pertains to the  $\alpha$ -cells with hyperpolarized  $V_{2h}$  (cells in shaded region in a(i)). One-way ANOVA; n.s., not significant,  $*p < 0.05$ ,  $**p < 0.01$ . (Online version in colour.)

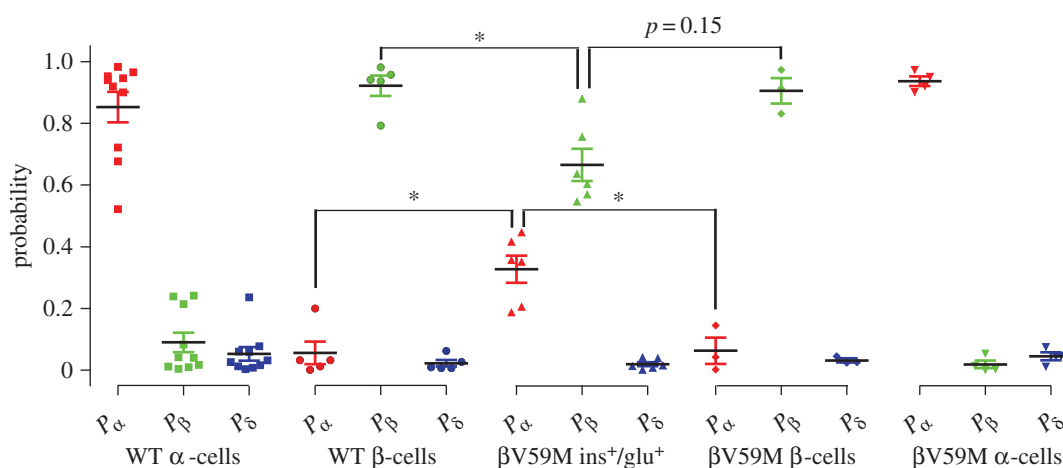


**Figure 8.** The multinomial logistic regression model can predict cell type in an animal strain of diabetes. Cell type was predicted for cells recorded from an animal with a hyperglycaemic phenotype (BV59M) and wild-type controls (WT). The model outputted the probability that each cell is an  $\alpha$ -cell ( $P_\alpha$ ),  $\beta$ -cell ( $P_\beta$ ) or  $\delta$ -cell ( $P_\delta$ ), from which the cell type predicted by the model could be determined. Cells that stained double positive for insulin and glucagon ( $\text{ins}^+/\text{glu}^+$ ) had a larger  $P_\alpha$  and smaller  $P_\beta$  than  $\beta$ -cells from WT and BV59M, suggesting that these cells had both  $\alpha$ - and  $\beta$ -cell electrophysiological properties. One-way ANOVA,  $*p < 0.05$ . (Online version in colour.)

( $P_\alpha = 0.86 \pm 0.05$ ) correctly. In BV59M mice, the model correctly identified all three  $\beta$ -cells ( $P_\beta = 0.91 \pm 0.04$ ) and four  $\alpha$ -cells ( $P_\alpha = 0.94 \pm 0.02$ ). The remaining six recordings from BV59M mice were revealed (by immunocytochemical staining)

to be from cells co-expressing insulin and glucagon ( $\text{ins}^+/\text{glu}^+$ ). The model identified all of these cells as  $\beta$ -cells ( $P_\beta = 0.67 \pm 0.05$ ). The probability that these cells were  $\alpha$ -cells ( $P_\alpha = 0.37 \pm 0.05$ ), as predicted by the model, was significantly

larger than the probability that  $\beta$ -cells from WT ( $P_{\alpha} = 0.06 \pm 0.04$ ;  $p = 0.022$ ) or  $\beta V59M$  ( $P_{\alpha} = 0.07 \pm 0.04$ ;  $p = 0.15$ ) mice were identified as  $\alpha$ -cells by the model. Furthermore, the model was less certain that these  $\beta V59M$   $ins^{+}/glu^{+}$  cells were  $\beta$ -cells;  $P_{\beta}$  in  $\beta V59M$   $ins^{+}/glu^{+}$  cells was smaller than in WT ( $p = 0.019$ ) and  $\beta V59M$  ( $p = 0.04$ )  $\beta$ -cells. Therefore, although the model predicted these six  $\beta V59M$   $ins^{+}/glu^{+}$  cells to be  $\beta$ -cells, it also revealed that they had ' $\alpha$ -cell-like' electrophysiological properties.

## 4. Discussion

Here we have quantified numerous electrophysiological variables in  $\alpha$ -,  $\beta$ - and  $\delta$ -cells from intact mouse islets. Our study highlights the perils of using a single electrophysiological variable to distinguish cell type and demonstrates that some established methods for functional identifying cell type are misleading (figures 1–4). We show, by constructing a multinomial logistic regression model (figure 6), that multiple electrophysiological variables can be used to predict islet cell type with 94% accuracy. The mathematical model was also able to identify cells from a diabetic mouse, and could distinguish cells in this mouse that were positive for both insulin and glucagon (figure 8).

### 4.1. Functionally identifying islet cell type based on a few electrophysiological properties

When recording membrane potential in the perforated patch-clamp configuration, the electrical activity of the cell in response to application of glucose is one method by which cell identity can be alluded to. The aim of this study was to provide a tool for accurately identifying cell type when membrane potential recording is not required or cannot be used (namely in voltage-clamp experiments under the standard whole-cell configuration).

Under the standard whole-cell configuration,  $\alpha$ -,  $\beta$ - and  $\delta$ -cells in mouse islets are known to exhibit electrophysiological properties that differ. These properties are often used to functionally identify the cell type [11,13,29,31,34–36,39–42,44,46–48,50,61]. For example, an electrophysiological feature that is commonly employed to distinguish cell type is the cell capacitance [3,13,35–41,43,44], which is largest in  $\beta$ -cells. Some studies have employed a criterion based on cell capacitance to distinguish  $\beta$ -cells from non- $\beta$ -cells [13,34,42]. However, we show that functionally identifying  $\beta$ -cells from non- $\beta$ -cells using cell capacitance is unreliable (figure 5*a,b*). Criteria based on cell capacitance alone may moderately enrich the cell type of interest, but will significantly reduce the sample size. Thus, even if subsequent criteria are applied (e.g. pertaining to  $Na^{+}$  current properties; see Rolland *et al.* [42]), the dataset will already be considerably reduced in size and not representative of the population. Furthermore, although our large dataset demonstrated many differences in electrophysiological properties across cell type, no single feature was able to distinguish islet cell type (table 2). A better method of identifying islet cell type is therefore required.

### 4.2. A multinomial logistic regression model for identifying islet cell type

To determine whether the electrophysiological features we measured could, collectively, be used to predict islet cell

type, we constructed a multinomial logistic regression model. This model was able to predict islet cell type with 94% accuracy (figure 6). It requires only a few standard electrophysiological variables as input. Its accuracy and speed could aid online identification of cell type and can replace the lengthy immunocytochemical and imaging procedures. This model demonstrated that  $Na^{+}$  current variables, the input resistance ( $1/G$ ) and cell capacitance are significant predictors of cell type, when important experimental confounders (e.g. access resistance and leak current) are controlled for. Interestingly, the model revealed that the leak current—an experimental confounder—is a significant predictor of cell type (table 4). It is therefore important to consider such experimental confounders when using electrophysiological variables to identify cell type.

For each recorded cell, the model generated probabilities  $P_{\alpha}$ ,  $P_{\beta}$  and  $P_{\delta}$ —the maximum of which yielded the cell type predicted by the model. The model could correctly identify cell type in mice with a diabetic phenotype [54] and identify cells that were positive for both insulin and glucagon. It may therefore help to understand the electrophysiological properties of cells undergoing reprogramming [62].

### 4.3. A-type $K^{+}$ current (transient outward current) as an identifier of cell type

The presence/absence of an A-current has been used in many studies as an identifying feature for  $\alpha$ -cells/ $\delta$ -cells, respectively [29,31,38,46–48]. Our analysis of a large sample of cells revealed that the notion that the A-current is an identifying feature of  $\alpha$ -cells is false (figure 4). We demonstrate that it is a feature of both  $\delta$ -cells (67% of  $\delta$ -cells exhibited a transient outward current) and  $\alpha$ -cells (20%; figure 4*c*). This is supported by transcriptome data from DiGrucchio *et al.* [59] that report expression of genes encoding A-type  $K^{+}$  channels in both  $\alpha$ - and  $\delta$ -cells (figure 4*d*) [59]. *KCNA4* and *KCND2* are preferentially expressed in  $\delta$ -cells, and *KCND1* and *KCND3* exhibit similar levels of expression in  $\alpha$ - and  $\delta$ -cells. Similarly, Adriaenssens *et al.* [56] recently reported genes differentially expressed between  $\alpha$ -,  $\beta$ - and  $\delta$ -cells; genes encoded by A-type channels were not found to exhibit significant expression changes between  $\alpha$ - and  $\delta$ -cells [56]. In conclusion, the presence of an A-type current is not unique to  $\alpha$ -cells, and should therefore be avoided as an identifier of cell type.

How do we reconcile this fact with the observation that 4-aminopyridine (4-AP) reduces glucagon secretion in mouse islets [49]? First, although 4-AP is traditionally seen as a blocker of A-type  $K^{+}$  channels [63], it is not selective for  $K^{+}$  channels that inactivate; it blocks both slowly inactivating and non-inactivating  $K^{+}$  currents of delayed rectifier type, including *Shaker* family members Kv1.1 [64], Kv1.2 [65], Kv1.3 [66], Kv1.5 [67,68] and Kv1.6 [69], as well as *Shab*-related Kv2.1 and *Shaw*-related Kv3.1 [70]. Secondly, if, as our analysis suggests, the A-type current is actually a fingerprint of  $\delta$ -cells, then blockade of this current will increase action potential width in  $\delta$ -cells, facilitating somatostatin release. This may decrease glucagon secretion via paracrine inhibition of  $\alpha$ -cells [71].

### 4.4. Improved conductance-based models of $\alpha$ -cells

To demonstrate the importance of our improved characterization of the electrophysiological properties of  $\alpha$ - and  $\delta$ -cells,

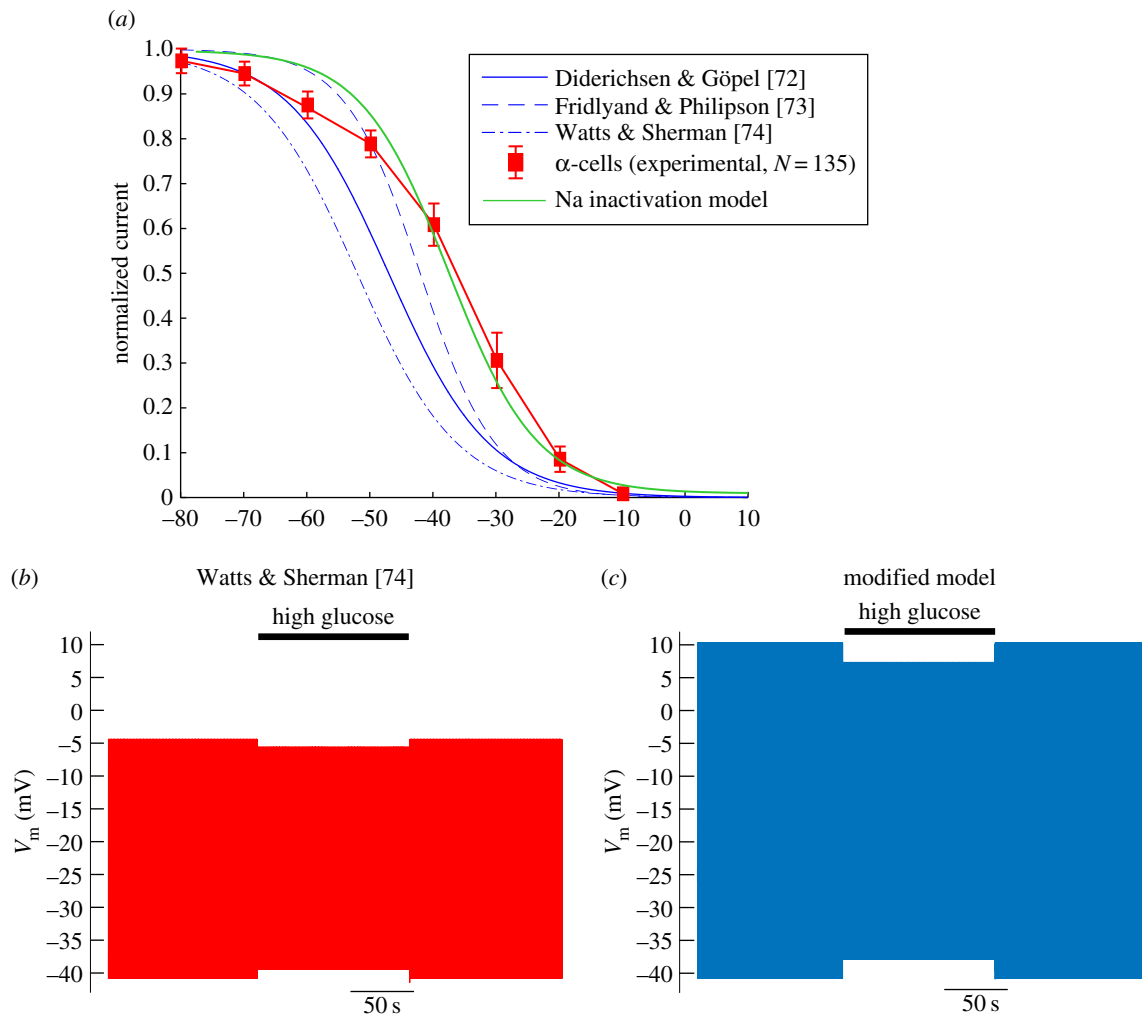


**Figure 9.** Modifying a conductance-based model of an  $\alpha$ -cell improves the fit to experimental data. (a) Steady-state  $\text{Na}^+$  current inactivation in three conductance-based models of  $\alpha$ -cells [72–74],  $N = 141$  experimentally recorded  $\alpha$ -cells, and our modified model ( $\text{Na}^+$  inactivation model). Our modified model can be seen to fit the experimental data well. We simulated the model of (b) Watts & Sherman [74] and (c) our modified model under conditions of high glucose (decreased  $G_{\text{KATP}}$ ; black line). Our model produced a 6.1 mV change in action potential height, as seen experimentally [11]. In comparison, the model of Watts & Sherman [74] produced moderate changes in action potential height (2.5 mV) and doublet spikes in response to high glucose. (Online version in colour.)

we used our findings to develop models of the electrical activity in these cell types (figures 9 and 10).

#### 4.5. An improved conductance-based model of $\alpha$ -cell electrical activity

Conductance-based mathematical models of the electrical activity of  $\alpha$ -cells have provided us with invaluable insights into the mechanisms regulating glucagon secretion [72–75]. However, parameters used in these models were based on presumptive  $\alpha$ -cells identified by traditional electrophysiological criteria [3,29,31,35,38,46], which we have shown here to be inaccurate. The parameters used in these models were therefore not always correct. The recent model of Watts & Sherman [74] includes an A-type  $\text{K}^+$  current which we demonstrate is present in 20% of  $\alpha$ -cells (figure 4). It also included  $\text{Na}^+$  current parameters that did not resemble our experimental dataset (figure 9a). Furthermore, the cell capacitance reported in previously published models was 5 pF [72–74], which does not resemble  $C_{\text{cell}}$  for  $\alpha$ -cells reported here ( $4.2 \pm 0.1$  pF; figure 1a) or previously [11,45]. These discrepancies may explain why the model of Watts & Sherman [74] produced a small decrease in spike height (2.45 mV) and doublet spikes during simulation of high-glucose conditions (figure 9b,c), a feature not seen experimentally [11]. We therefore modified this model in the light of

our findings (appendix C). When we removed the A-current, decreased  $C_{\text{cell}}$  to 4 pF and modified the  $\text{Na}^+$  current parameters in the model to fit our experimental data, the similarity between the model and the experimental data under simulated high-glucose improved. In particular, in low-glucose conditions, the spike height of the model action potential overshoot 0 mV and had an amplitude of more than 50 mV, as seen experimentally [11,52]. Moreover, in high-glucose conditions, the decrease in spike height was larger (6.1 mV), as observed experimentally [11]. These results do not disagree with the results produced from simulations of conductance-based models of  $\alpha$ -cells by Watts & Sherman [74]. In fact, we used the model by Watts & Sherman [74] as a starting model (as opposed to the other available models of  $\alpha$ -cells) because it correctly captures the phenomenological behaviour seen in the experimental data when high glucose is added. Our improvement of this model, based on our experimental findings, illustrates the importance of using reliable techniques for identifying cell type.

#### 4.6. An improved conductance-based model of $\delta$ -cell electrical activity

A conductance-based model of  $\delta$ -cell electrical activity calibrated against experimental data does not exist. Recently,

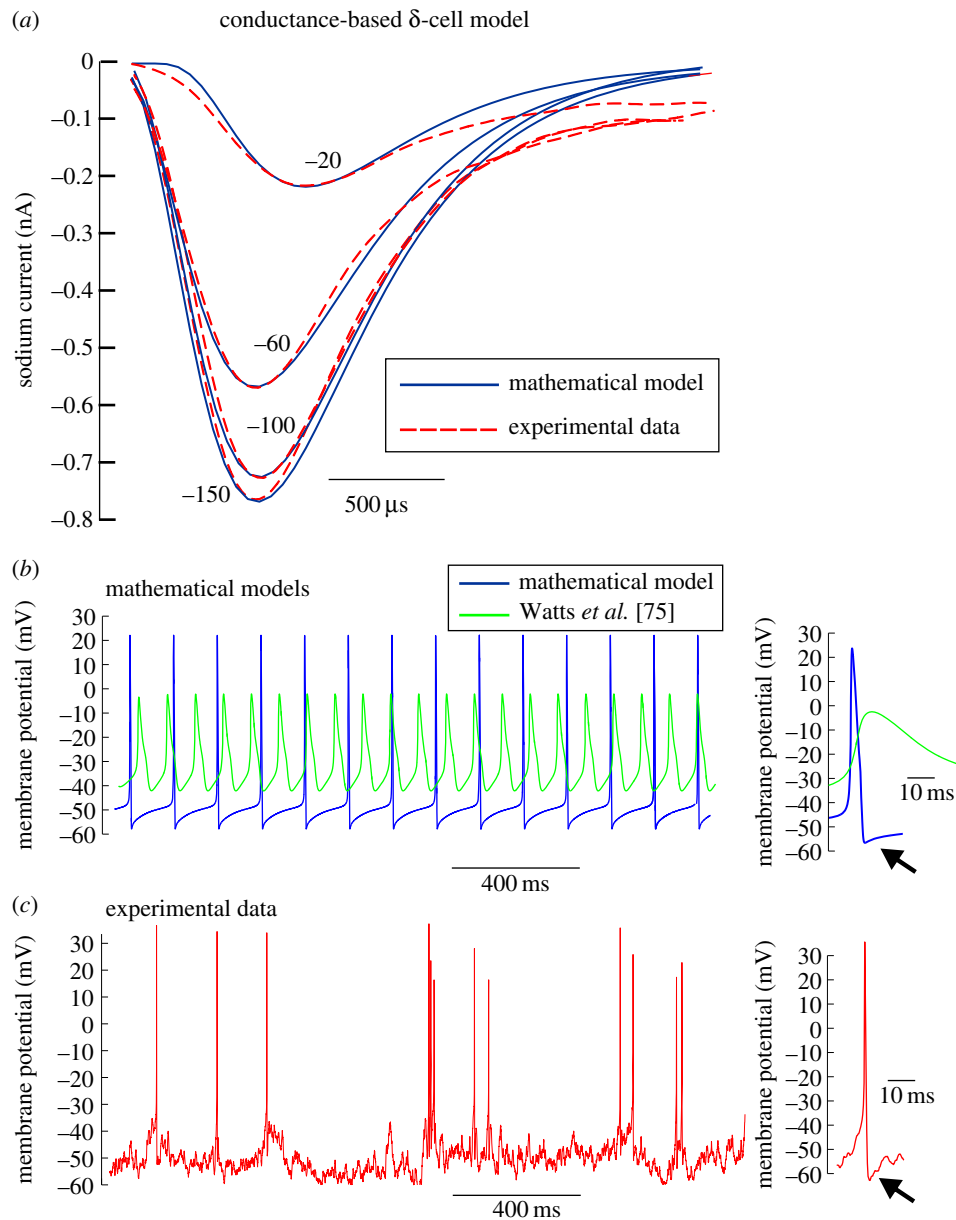


**Figure 10.** Modifying a conductance-based model of a  $\delta$ -cell improves the fit to experimental data. We used our large dataset to improve the fit of a conductance-based model of a  $\delta$ -cell to the experimental data. The  $\delta$ -cell model of Watts *et al.* [75] was used as the starting model. (a) The model was simulated under a  $\text{Na}^+$  current inactivation voltage-step protocol ( $V_{\text{cond}} = -180$  to  $20$  mV followed by a test pulse to  $0$  mV), and the evoked  $\text{Na}^+$  current in the model (solid) was compared with the inward current experimentally recorded from a  $\delta$ -cell under the same protocol (dashed). The  $\text{Na}^+$  current model parameters were then optimized by the method of Willms *et al.* [76], so that the model fitted the experimental data. The currents shown are in response to  $V_{\text{cond}} = -150$ ,  $-100$ ,  $-60$  and  $-20$  mV. (b) Spiking behaviour generated by the model of Watts *et al.* [75] with the reparametrized  $\text{Na}^+$  current model (as shown in a) and  $C_{\text{cell}} = 4$  pF was compared with the original, unaltered  $\delta$ -cell model by Watts *et al.* [75]. Note that action potentials evoked in the improved model overshoot  $0$  mV, have short duration and also have a pronounced after-hyperpolarization (arrows; owing to the A-type  $\text{K}^+$  current), as seen in the experimental action potentials recorded from a  $\delta$ -cell under the perforated patch-clamp configuration (c). (Online version in colour.)

Watts *et al.* [75] generated a conductance-based model of a  $\delta$ -cell for studying the dynamical interactions between cell types, but this was a modified version of an  $\alpha$ -cell model [75]. We therefore developed a model of  $\delta$ -cell electrical activity, constrained to our experimental data for  $\delta$ -cells (figure 10 and appendix C). The  $\text{Na}^+$  current kinetics in the model were fitted to experimental data from a  $\delta$ -cell recording by the improved parameter estimation method proposed by Willms *et al.* [76]. Given that our data demonstrate that  $\delta$ -cells have slow  $\text{Ca}^{2+}$  tail currents (figure 3) and A-currents (figure 4), T-type  $\text{Ca}^{2+}$  and A-type  $\text{K}^+$  currents were included in the model. These modifications produced a good fit between the model and experimental data in response to the  $\text{Na}^+$  inactivation protocol (from a single recording of a

$\delta$ -cell; figure 10a). We also changed  $C_{\text{cell}}$  in the model (from  $5$  to  $4$  pF) to fit the experimental data for  $\delta$ -cells ( $4.3 \pm 0.1$  pF,  $N = 91$ ; figure 1a). When the model was simulated under current clamp conditions, it produced large-amplitude spikes that overshoot  $0$  mV and had large after-hyperpolarizations (figure 10b). Similar spikes were seen experimentally using the perforated patch-clamp configuration (figure 10c).

#### 4.7. Future directions and conclusions

We have focused our model on characterizing islet cell type from recordings made from intact islets. Some studies, however, use dispersed islet cells. Our model was not tested against recordings from dispersed cells for two reasons.

First, cell identification by immunocytochemistry is straightforward in dispersed cells. Second, there is evidence that both cell size and  $\text{Na}^+$  current density are altered in dispersed islet cells [77].

$\alpha$ -,  $\beta$ - and  $\delta$ -cells in human islets possess very distinct electrophysiological features compared with their mouse counterparts [78–80]. Unlike the mouse, no functional identification exists for human cell type; patch-clamp recordings from human islets are rare. Therefore, identification of cell type demands successful immunocytochemical staining. The difficulties faced when studying the electrophysiological properties of human islet cells are reflected by the sample sizes (typically  $<10$  [78–80]). Furthermore, human islet function is very heterogeneous [11,81,82]. These obstacles have undoubtedly contributed to the slow progress in our understanding of the electrophysiological properties of each cell type in human islets, and how these properties correlate to the phenotype (e.g. non-diabetic/diabetic) of the donor.

The modelling process outlined in this study would also be helpful in the study of human islets. Such a model could be used to determine the key electrophysiological variables that identify cell type, making comprehensible the defining electrophysiological properties of these heterogeneous cells. It could also be used to predict the disease state (non-diabetic/diabetic) of a donor given a set of electrophysiological variables. Such a modelling procedure would illuminate which electrophysiological properties differ in diabetes, while correctly controlling for experimental confounders.

In conclusion, we have conducted a comprehensive analysis of the electrophysiological properties of islet cells traditionally used for identifying cell type, in a large population of recordings. We used this dataset to reveal which electrophysiological fingerprints were reliable for identifying cell type, and then constructed a logistic regression model that can be used to predict islet cell type with 94% accuracy. These data were successfully used to not only predict cell type in diabetic mouse models, but also improve conductance-based models of  $\alpha$ - and  $\delta$ -cells.

**Ethics.** All animal experiments were conducted in accordance with the UK Animals Scientific Procedures Act (1986) and University of Oxford ethical guidelines.

**Authors' contributions.** All authors had significant intellectual input into the study and gave final approval for publication. L.J.B.B. conceived the study design, drafted the manuscript, constructed and simulated the mathematical models and analysed the experimental and computational data. J.A.K. analysed the experimental data. E.V. and Q.Z. recorded the experimental data. Q.Z., F.M.A. and B.R. helped draft the manuscript. P.R. conceived the study design and helped draft the manuscript.

**Competing interests.** We have no competing interests.

**Funding.** L.J.B.B. is supported by a Sir Henry Wellcome Postdoctoral Fellowship (Wellcome Trust, 201325/Z/16/Z). Q.Z. holds an RD Lawrence Fellowship (Diabetes UK). J.A.K. and E.V. hold Wellcome Trust OXION PhD studentships. Financial support was also received from Wellcome Trust grant nos. 884655, 089795 and 095531. B.R. is supported by a Wellcome Trust Senior Research Fellowship in Basic Biomedical Science (100246/Z/12/Z), the British Heart Foundation Centre of Research Excellence in Oxford (RE/13/1/30181), an NC3R Infrastructure for Impact award (NC/P001076/1), an EPSRC Impact Acceleration Award (EP/K503769/1) and the ComBioMed project supported by the European Commission (grant agreement no. 675451). F.M.A. holds an ERC Advanced Investigator award (322620) and a Royal Society/Wolfson Merit Award.

**Acknowledgements.** We thank Dr Melissa Brereton for her help with the experimental mouse model of diabetes ( $\beta\text{V59M}$ ).

## Appendix A: electrophysiological variables quantified

Here we describe the experimental electrophysiological variables quantified from every recorded cell.

### A.1. Whole-cell conductance ( $G$ )

The reciprocal of the input resistance ( $1/R_{\text{input}}$ ), taken from the parameter window of the EPC-10, was computed to yield the whole-cell conductance ( $G$ ). This to a large extent reflects the  $K_{\text{ATP}}$ -channel conductance ( $G_{\text{KATP}}$ ).

### A.2. $\text{Na}^+$ current variables

Voltage-gated  $\text{Na}^+$  currents ( $I_{\text{Na}}$ ) exhibit distinct properties in  $\beta$ - and non- $\beta$ -cells; these are frequently used to functionally identify cell type [3,11,29,35,37–41,44–47,50]. We therefore sought to characterize these fingerprints in each cell recorded. Steady-state properties of  $I_{\text{Na}}$  were investigated by applying a 200 ms conditioning potential ( $V_{\text{cond}} = -180$  to 20 mV, 10 mV increments) followed by a 10 ms test pulse to 0 mV. Maximum  $\text{Na}^+$  current amplitude ( $I_{\text{max}}$ ) was taken as the peak current evoked following a conditioning pulse of  $V_{\text{cond}} = -180$  mV. For each conditioning potential, the peak current evoked during the test pulse ( $I$ ) was normalized by  $I_{\text{max}}$ . This yielded a sigmoid relationship, which represents the steady-state inactivation of the  $\text{Na}^+$  current ( $h_{\infty} = I/I_{\text{max}}$ ) as a function of  $V_{\text{cond}}$ . The data were then fitted with a single sigmoid,

$$h_{\infty}(V_{\text{cond}}) = \frac{1}{1 + \exp((V_{\text{cond}} - V_{2h})/k_h)},$$

in Matlab v. 6.1 (2000; The MathWorks, Natick, MA). The fit process yielded two biological parameters for inactivation: the half-inactivation ( $V_{2h}$ ) and the slope factor ( $k_h$ ). It also produced a goodness-of-fit ( $R^2$ ). Zhang *et al.* [45] recently demonstrated that  $h_{\infty}$  in  $\beta$ -cells exhibits a biphasic shape and fits well with a double sigmoid,

$$h_{\infty}(V_{\text{cond}}) = A_0 + A_1 \left[ \frac{A_2}{1 + \exp((V_{\text{cond}} - V_{2h,1})/k_{h,1})} + \frac{1 + A_2}{1 + \exp((V_{\text{cond}} - V_{2h,2})/k_{h,2})} \right].$$

We therefore fitted all data with both a double and single sigmoid function. The fit with the largest  $R^2$  was taken as the most appropriate fit for the  $h_{\infty}(V_{\text{cond}})$  data. If the fit was a double sigmoid, then the value of  $V_{2h}$  used to compare with other cell types was the most negative value out of  $V_{2h,1}$  and  $V_{2h,2}$ .

### A.3. Cell capacitance, $R_{\text{access}}$ and $I_{\text{leak}}$

$\alpha$ -,  $\beta$ - and  $\delta$ -cells differ in cell size and this is frequently used as an identifying feature for cell type [3,13,35–41,43,44]. A proxy for cell size (measurable during whole-cell patch-clamp recordings) is cell capacitance ( $C_{\text{cell}}$ ). This is taken as the slow component of the capacitive transient, as, after fast capacitance compensation for electrode capacitance, all remaining capacitive transients come from the cell capacitance [83].

The access (series) resistance ( $R_{\text{access}}$ ) was also recorded as this is a potential confounder of the recorded

electrophysiological properties of the cell [84,85]. Similarly, the leak current ( $I_{\text{leak}}$ ) was recorded.

#### A.4. Transient outward and slow tail currents

In some recordings, application of a conditioning potential  $V_{\text{cond}} < -70$  mV, followed by a test pulse to 0 mV, evoked a transient outward current that persisted in the presence of 20 mM TEA-Cl. This current, carried by  $K^+$  and putatively of A-type, has been used to identify  $\alpha$ -cells [29,31,38,46–48]. In each cell, we characterized whether such a current was present or absent (transient current = yes/no; table 1).

A current–voltage protocol was also applied to each cell recorded, to determine the peak currents elicited by voltage steps to different membrane potentials. Voltage steps of amplitude  $-100$  to  $30$  mV ( $10$  mV increments) were applied from a holding potential of  $-70$  mV, and the evoked current recorded. This peak current was recorded ( $I_{\text{max}70}$ ). In some cells, a slowly deactivating inward tail current (slow tail current) was observed on termination of the voltage step to  $30$  mV. This slow tail current, presumed to be a T-type  $\text{Ca}^{2+}$  current, has been used to identify islet cell type [29,31,38,46]. In each recorded cell, we characterized whether this slow tail current was present or absent (tail current = yes/no; table 1). As this characteristic is descriptive and subjective, we fitted a single exponential to the decay time course of this slow tail current; if the time constant of decay was more than  $1.5$  ms then a slow tail current was considered to be present (tail current = yes).

## Appendix B: multinomial logistic regression model for identifying islet cell type

### B.1. Multinomial logistic regression analysis

Our aim was to use the experimental variables calculated (table 1) to construct a regression model for predicting cell type ( $\alpha$ ,  $\beta$  or  $\delta$ ). Because the dependent variable is categorical with more than two levels, we fitted a multinomial logistic regression model to the experimental data. The benefit of this form of regression model is that it allows independent variables to be both categorical and continuous. It also accounts for experimental confounders [86] and how these influence identification of cell type. The model has the form

$$\left. \begin{aligned} \ln\left(\frac{P_{\alpha}}{1-P_{\alpha}}\right) &= B_{0\alpha} + X_1 B_{1\alpha} + \dots + X_i B_{i\alpha} \dots + X_n B_{n\alpha}, \\ \ln\left(\frac{P_{\beta}}{1-P_{\beta}}\right) &= B_{0\beta} + X_1 B_{1\beta} + \dots + X_i B_{i\beta} \dots + X_n B_{n\beta}. \end{aligned} \right\} \quad (\text{B1})$$

Here,  $B_{i\alpha}$  and  $B_{i\beta}$  are  $2(n+1)$  parameters determined by the modelling fitting process and  $X_i$  are the  $n$  independent variables (identifying features). For example, our model may include  $X_1 = V_{2h}$  and  $X_2 = C_{\text{cell}}$ . Given a cell and its set of values of  $X_i$ , the model produces  $P_{\alpha}$  and  $P_{\beta}$ —the probabilities that the cell is an  $\alpha$ -cell and  $\beta$ -cell, respectively. This model also yields the probability that a cell is a  $\delta$ -cell;  $P_{\delta} = 1 - P_{\alpha} - P_{\beta}$ . What remains to be outlined is how (i)  $B_{i\alpha}$  and  $B_{i\beta}$  are determined and (ii) the variables  $X_i$  are chosen.

### B.2. Model construction

In the model fitting process, parameter values ( $B_{i\alpha}$ ,  $B_{i\beta}$ ) were chosen so that they maximized the likelihood of observing

the sampled values  $X_i$  [87]. For the model fitting process,  $N = 175$  recordings made in mice with a normoglycaemic phenotype (60% of the normoglycaemic dataset) were used as the sample values, and the model was fitted to these samples (table 3). This dataset is referred to as the ‘model construction’ dataset. All logistic regression models presented were constructed using this dataset.

### B.3. Models with one independent variable

To understand whether a particular independent variable (e.g.  $X_1 = V_{2h}$ ) can alone identify cell type, equation (B1) was fitted to the experimental data with just this single independent variable. This model takes the form

$$\left. \begin{aligned} \ln\left(\frac{P_{\alpha}}{1-P_{\alpha}}\right) &= B_{0\alpha} + X_1 B_{1\alpha}, \\ \ln\left(\frac{P_{\beta}}{1-P_{\beta}}\right) &= B_{0\beta} + X_1 B_{1\beta}, \end{aligned} \right\} \quad (\text{B2})$$

where  $B_{0\alpha}$ ,  $B_{1\alpha}$ ,  $B_{0\beta}$  and  $B_{1\beta}$  are parameters determined by the fitting process and  $X_1$  is the independent variable of interest. This model can be used to understand how reliable  $X_1$  alone is at correctly identifying cell type.

### B.4. Model with more than one independent variable—the variable selection process

To understand whether the electrophysiological variables could be used together to accurately predict cell type, a forward-entry approach was taken. A variable was entered into the model as a new independent variable  $X_i$  if it significantly increased the maximum likelihood of observing the sampled values [87]. The variables considered for this process are precisely those described above (table 1). A backward-elimination method was also applied to test stability of the variable selection process.

Certain variables were forced to be in the model. Experimental confounders were accounted for by inclusion in the initial model [86]. Because  $R_{\text{access}}$  can influence the observed current–voltage relationship and the temporal resolution of recorded currents [84,85], this variable was considered as an experimental confounder and forced to be in the model. For similar reasons, multiplicative variables were included in the variable selection process;  $R_{\text{access}} \cdot I_{\text{max}}$ ,  $R_{\text{access}} \cdot V_{2h}$  and  $R_{\text{access}} \cdot k_h$  were subjected to maximum-likelihood criteria for inclusion in the model.  $I_{\text{leak}}$ , which is a measure of the seal quality, was forced to be in the model. The strain of the animal from which the cell recording was taken was considered as experimental confounders (influencing cell type). This categorical variable was not forced to be in the model but instead subjected to the aforementioned maximum-likelihood criteria. Many studies report  $I_{\text{max}}$  normalized to  $C_{\text{cell}}$  because this can bias the current amplitude; the larger the cell area, the larger the current recorded. We could account for this in the model by including the variable  $C_{\text{cell}} \cdot I_{\text{max}}$  in the modelling process and seeing whether this explained any variance in cell type. Two intracellular solutions were used for recording (solutions 1 and 2). As the solution used may influence the magnitude of the outward currents observable, and outward (namely A type) currents are used to identify cell type, we included the variable intracellular solution (solution 1/solution 2) as a confounder in the model.

The final model from this process was used to calculate the probability that any given cell (with sample values  $X_i$  for  $i = 0, \dots, n$ ) is an  $\alpha$ -cell ( $P_\alpha$ ),  $\beta$ -cell ( $P_\beta$ ) or  $\delta$ -cell ( $P_\delta$ ). The maximum of these three computed probabilities determines the cell type predicted by the model and can be compared with the observed cell type (confirmed by immunocytochemistry).

## B.5. Model validation

Following the model construction process, the model was validated. To ensure that the model fit is generalizable to other datasets, a second dataset (distinct from the model construction dataset) was used. This 'model validation' dataset consisted of the remaining  $N = 113$  cell recordings made from mice with a normoglycaemic phenotype (40% of the normoglycaemic dataset; table 3). For each cell recording (with experimental variables  $X_i$ ), the values  $X_i$  were entered into equation (B 1) and the probabilities ( $P_\alpha$ ,  $P_\beta$ ,  $P_\delta$ ) computed. The cell type predicted by the model could then be compared with the observed cell type.

## Appendix C: conductance-based models of electrical activity

### C.1. Conductance-based models of $\alpha$ -cells

We studied how any discrepancies in the identifying features of  $\alpha$ -cells would change the behaviour of previously published conductance-based models of  $\alpha$ -cells (which have relied on these identifying features to constrain model parameters). To do this, we used the recent model by Watts & Sherman [74]. The unmodified model is

$$C_{\text{cell}} \frac{dV}{dt} = -(I_{\text{CaL}} + I_{\text{CaN}} + I_{\text{CaT}} + I_{\text{Na}} + I_{\text{K}} + I_{\text{KATP}} + I_{\text{KA}} + I_{\text{L}} + I_{\text{SOC}}),$$

where  $C_{\text{cell}}$  is the cell capacitance;  $I_{\text{CaL}}$ ,  $I_{\text{CaN}}$  and  $I_{\text{CaT}}$  are L-, N- and T-type voltage-dependent  $\text{Ca}^{2+}$  currents, respectively;  $I_{\text{Na}}$  is a voltage-dependent  $\text{Na}^+$  current;  $I_{\text{K}}$  is a delayed rectifier  $\text{K}^+$  current;  $I_{\text{KA}}$  is an A-type voltage-dependent  $\text{K}^+$  current;  $I_{\text{K(ATP)}}$  is an ATP-sensitive  $\text{K}^+$  current;  $I_{\text{L}}$  is a leak current; and  $I_{\text{SOC}}$  is a store-operated  $\text{Ca}^{2+}$  current. A full description of this model can be found in Watts & Sherman [74] and the model code can be obtained from GitHub ([https://github.com/IsletCellType/IsletCellType\\_GitHub](https://github.com/IsletCellType/IsletCellType_GitHub)).

### C.2. Conductance-based models of $\delta$ -cells

Similarly, we studied how any discrepancies in the identifying features of  $\delta$ -cells would change the behaviour of previously published conductance-based models of  $\delta$ -cells (which have relied on these identifying features to constrain model parameters). To do this, we used the recent model by Watts *et al.* [75]. The unmodified model is

$$C_{\text{cell}} \frac{dV}{dt} = -(I_{\text{CaL}} + I_{\text{CaN}} + I_{\text{Na}} + I_{\text{K}} + I_{\text{KATP}} + I_{\text{KA}} + I_{\text{L}}),$$

where  $C_{\text{cell}}$  is the cell capacitance;  $I_{\text{CaL}}$  and  $I_{\text{CaN}}$  are the L- and N-type voltage-dependent  $\text{Ca}^{2+}$  currents, respectively;  $I_{\text{Na}}$  is a voltage-dependent  $\text{Na}^+$  current;  $I_{\text{K}}$  is a delayed rectifier  $\text{K}^+$  current;  $I_{\text{KA}}$  is an A-type voltage-dependent  $\text{K}^+$  current;  $I_{\text{K(ATP)}}$  is an ATP-sensitive  $\text{K}^+$  current; and  $I_{\text{L}}$  is a leak current. The GABA current was excluded from the model as we were not modelling paracrine signalling. The parameter values of  $I_{\text{K}}$ ,  $I_{\text{K(ATP)}}$ ,  $I_{\text{KA}}$  and  $I_{\text{L}}$  were left unmodified. The parameter values of  $I_{\text{Na}}$  were fitted to experimental data by the process described by Willms *et al.* [76]. The only further modification to this model was that the time constants of the voltage-gated  $\text{Ca}^{2+}$  channels were decreased, because action potentials generated by the model were seen to be too broad in comparison with experimental data. This model is available online at GitHub ([https://github.com/IsletCellType/IsletCellType\\_GitHub](https://github.com/IsletCellType/IsletCellType_GitHub)).

## References

- Steiner DJ, Kim A, Miller K, Hara M. 2010 Pancreatic islet plasticity: interspecies comparison of islet architecture and composition. *Islets* **2**, 135–145. (doi:10.4161/isl.2.3.11815)
- Orci L. 1982 Macro- and micro-domains in the endocrine pancreas. *Diabetes* **31**, 538–565. (doi:10.2337/diab.31.6.538)
- Gopel SO, Kanno T, Barg S, Rorsman P. 2000 Patch-clamp characterisation of somatostatin-secreting cells in intact mouse pancreatic islets. *J. Physiol.* **528**, 497–507. (doi:10.1111/j.1469-7793.2000.00497.x)
- Gromada J, Franklin I, Wollheim CB. 2007 Alpha-cells of the endocrine pancreas: 35 years of research but the enigma remains. *Endocr. Rev.* **28**, 84–116. (doi:10.1210/er.2006-0007)
- Meissner HP, Schmeltz H. 1974 Membrane potential of beta-cells in pancreatic islets. *Pflugers Arch.* **351**, 195–206. (doi:10.1007/BF00586918)
- Williams RH, Ensink JW. 1966 Secretion, fates and actions of insulin and related products. *Diabetes* **15**, 623–654. (doi:10.2337/diab.15.9.623)
- Unger RH. 1985 Glucagon physiology and pathophysiology in the light of new advances. *Diabetologia* **28**, 574–578. (doi:10.1007/BF00281991)
- Hauge-Evans AC, King AJ, Carmignani D, Richardson CC, Robinson ICAF, Low MJ, Christie MR, Persaud SJ, Jones PM. 2009 Somatostatin secreted by islet delta-cells fulfills multiple roles as a paracrine regulator of islet function. *Diabetes* **58**, 403–411. (doi:10.2337/db08-0792)
- Guillausseau PJ, Meas T, Virally M, Laloi-Michelin M, Medeau V, Kevorkian JP. 2008 Abnormalities in insulin secretion in type 2 diabetes mellitus. *Diabetes Metab.* **34**(Suppl. 2), S43–S48. (doi:10.1016/S1262-3636(08)73394-9)
- Unger RH, Cherrington AD. 2012 Glucagonocentric restructuring of diabetes: a pathophysiologic and therapeutic makeover. *J. Clin. Invest.* **122**, 4–12. (doi:10.1172/JCI60016)
- Zhang Q *et al.* 2013 Role of KATP channels in glucose-regulated glucagon secretion and impaired counterregulation in type 2 diabetes. *Cell Metab.* **18**, 871–882. (doi:10.1016/j.cmet.2013.10.014)
- Huang YC, Rupnik MS, Karimian N, Herrera PL, Gilon P, Feng ZP, Gaisano HY. 2013 *In situ* electrophysiological examination of pancreatic alpha cells in the streptozotocin-induced diabetes model, revealing the cellular basis of glucagon hypersecretion. *Diabetes* **62**, 519–530. (doi:10.2337/db11-0786)
- Guo JH *et al.* 2014 Glucose-induced electrical activities and insulin secretion in pancreatic islet beta-cells are modulated by CFTR. *Nat. Commun.* **5**, 4420. (doi:10.1038/ncomms5420)
- Ashcroft FM, Rorsman P. 2012 Diabetes mellitus and the beta cell: the last ten years. *Cell* **148**, 1160–1171. (doi:10.1016/j.cell.2012.02.010)
- Baetens D, Malaisse-Lagae F, Perrelet A, Orci L. 1979 Endocrine pancreas: three-dimensional reconstruction shows two types of islets of Langerhans. *Science* **206**, 1323–1325. (doi:10.1126/science.390711)
- Seino S, Shibasaki T, Minami K. 2011 Dynamics of insulin secretion and the clinical implications for

- obesity and diabetes. *J. Clin. Invest.* **121**, 2118–2125. (doi:10.1172/JCI45680)
17. Remedi MS, Nichols CG. 2009 Hyperinsulinism and diabetes: genetic dissection of beta cell metabolism-excitation coupling in mice. *Cell Metab.* **10**, 442–453. (doi:10.1016/j.cmet.2009.10.011)
  18. Ashcroft FM, Proks P, Smith PA, Ammala C, Bokvist K, Rorsman P. 1994 Stimulus-secretion coupling in pancreatic beta cells. *J. Cell Biochem.* **55**(Suppl.), 54–65. (doi:10.1002/jcb.240550007)
  19. Gylfe E, Gilon P. 2014 Glucose regulation of glucagon secretion. *Diabetes Res. Clin. Pract.* **103**, 1–10. (doi:10.1016/j.diabetes.2013.11.019)
  20. Gylfe E. 2013 Glucose control of glucagon secretion: there is more to it than K-ATP channels. *Diabetes* **62**, 1391–1393. (doi:10.2337/db13-0193)
  21. Cheng-Xue R, Gomez-Ruiz A, Antoine N, Noel LA, Chae HY, Ravier MA, Chimienti F, Schuit FC, Gilon P. 2013 Tolbutamide controls glucagon release from mouse islets differently than glucose: involvement of K(ATP) channels from both alpha-cells and delta-cells. *Diabetes* **62**, 1612–1622. (doi:10.2337/db12-0347)
  22. Van De Winkel M, Pipeleers D. 1983 Autofluorescence-activated cell sorting of pancreatic islet cells: purification of insulin-containing B-cells according to glucose-induced changes in cellular redox state. *Biochem. Biophys. Res. Commun.* **114**, 835–842. (doi:10.1016/0006-291X(83)90857-4)
  23. Bloc A, Cens T, Cruz H, Dunant Y. 2000 Zinc-induced changes in ionic currents of clonal rat pancreatic cells: activation of ATP-sensitive K<sup>+</sup> channels. *J. Physiol.* **529**, 723–734. (doi:10.1111/j.1469-7793.2000.00723.x)
  24. Franklin I, Gromada J, Gjinovci A, Theander S, Wollheim CB. 2005 Beta-cell secretory products activate alpha-cell ATP-dependent potassium channels to inhibit glucagon release. *Diabetes* **54**, 1808–1815. (doi:10.2337/diabetes.54.6.1808)
  25. Kawamori D *et al.* 2009 Insulin signaling in alpha cells modulates glucagon secretion *in vivo*. *Cell Metab.* **9**, 350–361. (doi:10.1016/j.cmet.2009.02.007)
  26. Ravier MA, Rutter GA. 2005 Glucose or insulin, but not zinc ions, inhibit glucagon secretion from mouse pancreatic alpha-cells. *Diabetes* **54**, 1789–1797. (doi:10.2337/diabetes.54.6.1789)
  27. Strowski MZ, Parmar RM, Blake AD, Schaeffer JM. 2000 Somatostatin inhibits insulin and glucagon secretion via two receptor subtypes: an *in vitro* study of pancreatic islets from somatostatin receptor 2 knockout mice. *Endocrinology* **141**, 111–117. (doi:DOI 10.1210/en.141.1.111)
  28. Shuai H, Xu Y, Yu Q, Gylfe E, Tengholm A. 2016 Fluorescent protein vectors for pancreatic islet cell identification in live-cell imaging. *Pflugers Arch.* **468**, 1765–1777. (doi:10.1007/s00424-016-1864-z)
  29. Leung YM, Ahmed I, Sheu L, Tsushima RG, Diamant NE, Hara M, Gaisano HY. 2005 Electrophysiological characterization of pancreatic islet cells in the mouse insulin promoter-green fluorescent protein mouse. *Endocrinology* **146**, 4766–4775. (doi:10.1210/en.2005-0803)
  30. Hara M, Wang X, Kawamura T, Bindokas VP, Dizon RF, Alcoser SY, Magnuson MA, Bell GI. 2003 Transgenic mice with green fluorescent protein-labeled pancreatic beta-cells. *Am. J. Physiol. Endocrinol. Metab.* **284**, E177–E183. (doi:10.1152/ajpendo.00321.2002)
  31. Leung YM, Ahmed I, Sheu L, Gao X, Hara M, Tsushima RG, Diamant NE, Gaisano HY. 2006 Insulin regulates islet alpha-cell function by reducing KATP channel sensitivity to adenosine 5'-triphosphate inhibition. *Endocrinology* **147**, 2155–2162. (doi:10.1210/en.2005-1249)
  32. Quoix N, Cheng-Xue R, Guiot Y, Herrera PL, Henquin JC, Gilon P. 2007 The GluCre-ROSA26YFP mouse: a new model for easy identification of living pancreatic alpha-cells. *FEBS Lett.* **581**, 4235–4240. (doi:10.1016/j.febslet.2007.07.068)
  33. Quoix N, Cheng-Xue R, Mattart L, Zeinoun Z, Guiot Y, Beauvois MC, Henquin JC, Gilon P. 2009 Glucose and pharmacological modulators of ATP-sensitive K<sup>+</sup> channels control [Ca<sup>2+</sup>]<sub>i</sub> by different mechanisms in isolated mouse alpha-cells. *Diabetes* **58**, 412–421. (doi:10.2337/db07-1298)
  34. Andersson SA, Pedersen MG, Vikman J, Eliasson L. 2011 Glucose-dependent docking and SNARE protein-mediated exocytosis in mouse pancreatic alpha-cell. *Pflugers Arch.* **462**, 443–454. (doi:10.1007/s00424-011-0979-5)
  35. Barg S, Galvanovskis J, Gopel SO, Rorsman P, Eliasson L. 2000 Tight coupling between electrical activity and exocytosis in mouse glucagon-secreting alpha-cells. *Diabetes* **49**, 1500–1510. (doi:10.2337/diabetes.49.9.1500)
  36. Best L, Davies S, Brown PD. 2004 Tolbutamide potentiates the volume-regulated anion channel current in rat pancreatic beta cells. *Diabetologia* **47**, 1990–1997. (doi:10.1007/s00125-004-1559-4)
  37. Gopel S, Kanno T, Barg S, Galvanovskis J, Rorsman P. 1999 Voltage-gated and resting membrane currents recorded from B-cells in intact mouse pancreatic islets. *J. Physiol.* **521**, 717–728. (doi:10.1111/j.1469-7793.1999.00717.x)
  38. Gopel SO, Kanno T, Barg S, Weng XG, Gromada J, Rorsman P. 2000 Regulation of glucagon release in mouse-cells by KATP channels and inactivation of TTX-sensitive Na<sup>+</sup> channels. *J. Physiol.* **528**, 509–520. (doi:10.1111/j.1469-7793.2000.00509.x)
  39. Houamed KM, Sweet IR, Satin LS. 2010 BK channels mediate a novel ionic mechanism that regulates glucose-dependent electrical activity and insulin secretion in mouse pancreatic beta-cells. *J. Physiol.* **588**, 3511–3523. (doi:10.1113/jphysiol.2009.184341)
  40. Huang YC, Rupnik M, Gaisano HY. 2011 Unperturbed islet alpha-cell function examined in mouse pancreas tissue slices. *J. Physiol.* **589**, 395–408. (doi:10.1113/jphysiol.2010.200345)
  41. MacDonald PE, De Marinis YZ, Ramracheya R, Salehi A, Ma XS, Johnson PRV, Cox R, Eliasson L, Rorsman P. 2007 A K-ATP channel-dependent pathway within alpha cells regulates glucagon release from both rodent and human islets of Langerhans. *PLoS Biol.* **5**, 1236–1247. (doi:10.1371/journal.pbio.0050143)
  42. Rolland JF, Henquin JC, Gilon P. 2002 Feedback control of the ATP-sensitive K<sup>+</sup> current by cytosolic Ca<sup>2+</sup> contributes to oscillations of the membrane potential in pancreatic beta-cells. *Diabetes* **51**, 376–384. (doi:10.2337/diabetes.51.2.376)
  43. Vieira E, Salehi A, Gylfe E. 2007 Glucose inhibits glucagon secretion by a direct effect on mouse pancreatic alpha cells. *Diabetologia* **50**, 370–379. (doi:10.1007/s00125-006-0511-1)
  44. Xu E *et al.* 2006 Intra-islet insulin suppresses glucagon release via GABA-GABAA receptor system. *Cell Metab.* **3**, 47–58. (doi:10.1016/j.cmet.2005.11.015)
  45. Zhang Q *et al.* 2014 Na<sup>+</sup> current properties in islet α- and β-cells reflect cell-specific *Scn3a* and *Scn9a* expression. *J. Physiol.* **592**, 4677–4696. (doi:10.1113/jphysiol.2014.274209)
  46. Gopel S, Zhang Q, Eliasson L, Ma XS, Galvanovskis J, Kanno T, Salehi A, Rorsman P. 2004 Capacitance measurements of exocytosis in mouse pancreatic alpha-, beta- and delta-cells within intact islets of Langerhans. *J. Physiol. Lond.* **556**, 711–726. (doi:10.1113/jphysiol.2003.059675)
  47. Kanno T, Gopel SO, Rorsman P, Wakui M. 2002 Cellular function in multicellular system for hormone-secretion: electrophysiological aspect of studies on alpha-, beta- and delta-cells of the pancreatic islet. *Neurosci. Res.* **42**, 79–90. (doi:10.1016/S0168-0102(01)00318-2)
  48. Merino B, Alonso-Magdalena P, Lluesma M, Neco P, Gonzalez A, Marroqui L, Garcia-Arevalo M, Nadal A, Quesada I. 2015 Pancreatic alpha-cells from female mice undergo morphofunctional changes during compensatory adaptations of the endocrine pancreas to diet-induced obesity. *Sci. Rep.* **5**, 11622. (doi:10.1038/srep11622)
  49. Gromada J, Ma X, Hoy M, Bokvist K, Salehi A, Berggren PO, Rorsman P. 2004 ATP-sensitive K<sup>+</sup> channel-dependent regulation of glucagon release and electrical activity by glucose in wild-type and SUR1<sup>-/-</sup> mouse alpha-cells. *Diabetes* **53**(Suppl. 3), S181–S189. (doi:10.2337/diabetes.53.suppl\_3.S181)
  50. Tsiaze EB, Huang Y-C, Bombek LK, Yang S-B, Jevšek M, Seino S, Rupnik MS. 2012 Age-dependent changes in the exocytotic efficacy in Kir6.2 ablated mouse pancreatic β-cells. *Open J. Mol. Integr. Physiol.* **2**, 51–60. (doi:10.4236/ojimp.2012.23008)
  51. Allister EM *et al.* 2013 UCP2 regulates the glucagon response to fasting and starvation. *Diabetes* **62**, 1623–1633. (doi:10.2337/db12-0981)
  52. Dadi PK, Luo B, Vierra NC, Jacobson DA. 2015 TASK-1 potassium channels limit pancreatic alpha-cell calcium influx and glucagon secretion. *Mol. Endocrinol.* **29**, 777–787. (doi:10.1210/me.2014-1321)
  53. Vignali S, Leiss V, Karl R, Hofmann F, Welling A. 2006 Characterization of voltage-dependent sodium and calcium channels in mouse pancreatic A- and B-cells. *J. Physiol.* **572**, 691–706. (doi:10.1113/jphysiol.2005.102368)

54. Brereton MF *et al.* 2014 Reversible changes in pancreatic islet structure and function produced by elevated blood glucose. *Nat. Commun.* **5**, 4639. (doi:10.1038/ncomms5639)
55. Shibasaki T *et al.* 2007 Essential role of Epac2/Rap1 signaling in regulation of insulin granule dynamics by cAMP. *Proc. Natl Acad. Sci. USA* **104**, 19 333–19 338. (doi:10.1073/pnas.0707054104)
56. Adriaenssens AE, Svendsen B, Lam BY, Yeo GS, Holst JJ, Reimann F, Gribble FM. 2016 Transcriptomic profiling of pancreatic alpha, beta and delta cell populations identifies delta cells as a principal target for ghrelin in mouse islets. *Diabetologia* **59**, 2156–2165. (doi:10.1007/s00125-016-4033-1)
57. Sharpe D. 2015 Your chi-square test is statistically significant: now what? *Pract. Assess. Res. Eval.* **20**. See <http://pareonline.net/getvn.asp?v=20&n=8>.
58. Ermentrout B. 2002 *Simulating, analyzing, and animating dynamical systems: a guide to XPPAUT for researchers and students*. Philadelphia, PA: SIAM.
59. DiGruccio MR, Mawla AM, Donaldson CJ, Noguchi GM, Vaughan J, Cowing-Zitron C, van der Meulen T, Huisin MO. 2016 Comprehensive alpha, beta and delta cell transcriptomes reveal that ghrelin selectively activates delta cells and promotes somatostatin release from pancreatic islets. *Mol. Metab.* **5**, 449–458. (doi:10.1016/j.molmet.2016.04.007)
60. Menard S. 2011 Standards for standardized logistic regression coefficients. *Soc. Forces* **89**, 1409–1428. (doi:10.1093/sf/89.4.1409)
61. Eliasson L, Barg S, Gopel S, Kanno T, Renstrom E. 1999 Exocytosis in B-cells studied in intact mouse pancreatic islets by a combination of capacitance measurements and electron microscopy. *Diabetologia* **42**, A45. (doi:10.1007/s001250050111)
62. Migliorini A, Bader E, Lickert H. 2014 Islet cell plasticity and regeneration. *Mol. Metab.* **3**, 268–274. (doi:10.1016/j.molmet.2014.01.010)
63. Johnston D, Wu SM-S. 1995 *Foundations of cellular neurophysiology*. Cambridge, MA: MIT Press.
64. Stephens GJ, Garratt JC, Robertson B, Owen DG. 1994 On the mechanism of 4-aminopyridine action on the cloned mouse brain potassium channel mKv1.1. *J. Physiol.* **477**, 187–196. (doi:10.1113/jphysiol.1994.sp020183)
65. Russell SN, Publicover NG, Hart PJ, Carl A, Hume JR, Sanders KM, Horowitz B. 1994 Block by 4-aminopyridine of a Kv1.2 delayed rectifier K<sup>+</sup> current expressed in *Xenopus* oocytes. *J. Physiol.* **481**, 571–584. (doi:10.1113/jphysiol.1994.sp020464)
66. Comes N *et al.* 2013 The voltage-dependent K<sup>+</sup> channels Kv1.3 and Kv1.5 in human cancer. *Front. Physiol.* **4**, 283. (doi:10.3389/fphys.2013.00283)
67. Bouchard R, Fedida D. 1995 Closed- and open-state binding of 4-aminopyridine to the cloned human potassium channel Kv1.5. *J. Pharmacol. Exp. Ther.* **275**, 864–876.
68. Yamane T, Furukawa T, Hiraoka M. 1995 4-Aminopyridine block of the noninactivating cloned K<sup>+</sup> channel Kv1.5 expressed in *Xenopus* oocytes. *Am. J. Physiol.* **269**, H556–H564.
69. Glazebrook PA, Ramirez AN, Schild JH, Shieh CC, Doan T, Wible BA, Kunze DL. 2002 Potassium channels Kv1.1, Kv1.2 and Kv1.6 influence excitability of rat visceral sensory neurons. *J. Physiol.* **541**, 467–482. (doi:10.1113/jphysiol.2001.018333)
70. Kirsch GE, Drewe JA. 1993 Gating-dependent mechanism of 4-aminopyridine block in two related potassium channels. *J. Gen. Physiol.* **102**, 797–816. (doi:10.1085/jgp.102.5.797)
71. Gromada J, Hoy M, Buschard K, Salehi A, Rorsman P. 2001 Somatostatin inhibits exocytosis in rat pancreatic alpha-cells by G(i2)-dependent activation of calcineurin and depriving of secretory granules. *J. Physiol.* **535**, 519–532. (doi:10.1111/j.1469-7793.2001.00519.x)
72. Diderichsen PM, Göpel SO. 2006 Modelling the electrical activity of pancreatic  $\alpha$ -cells based on experimental data from intact mouse islets. *J. Biol. Phys.* **32**, 209–229. (doi:10.1007/s10867-006-9013-0)
73. Fridlyand LE, Philipson LH. 2012 A computational systems analysis of factors regulating alpha cell glucagon secretion. *Islets* **4**, 262–283. (doi:10.4161/isl.22193)
74. Watts M, Sherman A. 2014 Modeling the pancreatic alpha-cell: dual mechanisms of glucose suppression of glucagon secretion. *Biophys. J.* **106**, 741–751. (doi:10.1016/j.bpj.2013.11.4504)
75. Watts M, Ha J, Kimchi O, Sherman A. 2016 Paracrine regulation of glucagon secretion: the beta-alpha-delta model. *Am. J. Physiol. Endocrinol. Metab.* **310**, E597–E611. (doi:10.1152/ajpendo.00415.2015)
76. Willms AR, Baro DJ, Harris-Warrick RM, Guckenheimer J. 1999 An improved parameter estimation method for Hodgkin–Huxley models. *J. Comput. Neurosci.* **6**, 145–168. (doi:10.1023/A:1008880518515)
77. Briant L, Salehi A, Vergari E, Zhang Q, Rorsman P. 2016 Glucagon secretion from pancreatic alpha-cells. *Ups J. Med. Sci.* **121**, 113–119. (doi:10.3109/03009734.2016.1156789)
78. Braun M, Ramracheya R, Amisten S, Bengtsson M, Moritoh Y, Zhang Q, Johnson PR, Rorsman P. 2009 Somatostatin release, electrical activity, membrane currents and exocytosis in human pancreatic delta cells. *Diabetologia* **52**, 1566–1578. (doi:10.1007/s00125-009-1382-z)
79. Braun M, Ramracheya R, Bengtsson M, Zhang Q, Karanaukaite J, Partridge C, Johnson PR, Rorsman P. 2008 Voltage-gated ion channels in human pancreatic  $\beta$ -cells: electrophysiological characterization and role in insulin secretion. *Diabetes* **57**, 1618–1628. (doi:10.2337/db07-0991)
80. Ramracheya R, Ward C, Shigeto M, Walker JN, Amisten S, Zhang Q, Johnson PR, Rorsman P, Braun M. 2010 Membrane potential-dependent inactivation of voltage-gated ion channels in alpha-cells inhibits glucagon secretion from human islets. *Diabetes* **59**, 2198–2208. (doi:10.2337/db09-1505)
81. Dorrell C *et al.* 2016 Human islets contain four distinct subtypes of beta cells. *Nat. Commun.* **7**, 11756. (doi:10.1038/ncomms11756)
82. Wojtuszczyk A, Armanet M, Morel P, Berney T, Bosco D. 2008 Insulin secretion from human beta cells is heterogeneous and dependent on cell-to-cell contacts. *Diabetologia* **51**, 1843–1852. (doi:10.1007/s00125-008-1103-z)
83. Chen T-Y, Lin Y-F, Zheng Z. 2009 Electrophysiological measurements of membrane proteins. In *Fundamental concepts in biophysics* (ed. T Jue), pp. 111–137. Berlin, Germany: Springer.
84. Armstrong CM, Gilly WF. 1992 Access resistance and space clamp problems associated with whole-cell patch clamping. *Methods Enzymol.* **207**, 100–122. (doi:10.1016/0076-6879(92)07007-B)
85. Sigworth FJ. 1995 Electronic design of the patch clamp. In *Single-channel recording* (eds B Sakmann, E Neher), pp. 95–127. Berlin, Germany: Springer.
86. Stoltzfus JC. 2011 Logistic regression: a brief primer. *Acad. Emerg. Med.* **18**, 1099–1104. (doi:10.1111/j.1553-2712.2011.01185.x)
87. Czepl SA. 2002 Maximum likelihood estimation of logistic regression models: theory and implementation. See <http://czep.net/stat/mlr.pdf>.